Analysis of the Proton Transfer Bands in the Infrared Spectra of Linear N_2H^+…OC and N_2D^+…OC Complexes Using Electric Field-Driven Classical Trajectories

Dalton Boutwell, Onyi Okere, Oluwaseun Omodemi, Alexander Toledo, Antonio Barrios, Monique Olocha, Martina Kaledin*

Department of Chemistry & Biochemistry, Kennesaw State University, 370 Paulding Ave NW, Box # 1203, Kennesaw, GA 30144

ABSTRACT In this work we describe *ab initio* calculations and assignment of infrared (IR) spectra of hydrogen-bonded ion-molecular complexes that involve a fluxional proton: the linear N_2H^+…OC and N_2D^+…OC complexes. Given the challenges of describing fluxional proton dynamics and especially its IR activity, we use electric field-driven classical trajectories, i.e. the driven molecular dynamics (DMD) method that was developed by us in recent years and for similar applications, in conjunction with high level electronic structure theory. Namely, we present a modified and a numerically efficient implementation of DMD specifically for direct (or "on-the-fly") calculations, which we carry out at the MP2-F12/AVDZ level of theory for the potential energy surface (PES) and MP2/AVDZ for the dipole moment surfaces (DMS). Detailed analysis of the PES, DMS and the time-dependence of the first derivative of the DMS, referred to as the driving force, for the highly fluxional vibrations involving H^+/D^+ revealed that the strongly non-harmonic PES and non-linear DMS yield remarkably complex vibrational spectra. Interestingly, the classical trajectories reveal a doublet in the proton transfer part of the spectrum with the two peaks at 1800 and 1980 $cm.^{-1}$ We find that their shared intensity is due to a Fermi-like resonance interaction, within the classical limit, of the H^+ parallel stretch fundamental and an H^+ perpendicular bending overtone. This doublet is also observed in the deuterated species at 1360 and 1460 $cm.^{-1}$

Table of Content (TOC) figure

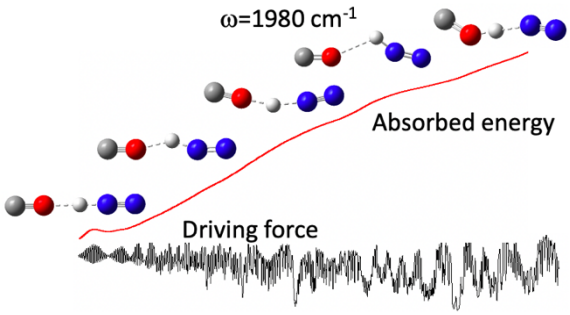

KEYWORDS Proton transfer, hydrogen-bonding interaction, driven molecular dynamics, normal mode analysis, combination bands, isotopic substitution, anharmonicity.

1. INTRODUCTION

Proton transport is an important process in acid-base environments, biological systems, and electrochemical devices. The mechanism of proton transport in hydrogen-bonded systems has attracted much attention in recent years.[1-4] Proton transfer involves the motion of the lightest atom and therefore induces considerable quantum effects, such as tunneling, and also significant anharmonic motion, and strong non-harmonic (cubic, quartic, etc.) coupling between a wide range of vibrational modes,[5-7] including low-frequency modes,[4] resulting in a very complicated vibrational structure. One of the most important unsolved spectroscopic problems involving small molecules is the IR spectrum of CH_5^+, the protonated methane.[8] For these reasons, the approaches based on the harmonic approximation of the potential energy surface around a single minimum (and the linear approximation of the dipole), such as the normal mode analysis (NMA), cannot properly describe the intrinsically non-harmonic proton dynamics. On the other hand, the strong non-harmonic effects can be partially described by performing classical molecular dynamics (MD) simulations,[5,9] and more comprehensively by quantum mechanical time-independent[4,6,7] or time-dependent calculations.[10-12] In the present work, we continue to investigate the facility of driven molecular dynamics (DMD) in characterizing infrared spectra of systems with a fluxional proton. A brief review of our earlier efforts and the pertinent ones of other investigators is given below.

Interstellar clouds contain a plethora of clusters of molecules and ions that exist in a variety of forms, particularly, protonated clusters of first row elements that exhibit intense vibrational transitions owing to the fluxionality of a shared proton. Recently, linear protonated complexes from a combination of C, N, and O atoms have attracted major attention due to their importance in biological processes, atmospheric chemistry and possible presence in the interstellar media.[13-27] Ion molecular reactions involving N_2H^+, HCO^+, and COH^+ with CO and N_2, which are common

interstellar species, have likewise attracted attention in recent years.[28-34] The so-called 57-mass protonated complexes contain isoelectronic diatomics N_2 and CO and a proton, H^+ in various configurations. Our work,[13] among that of others,[14-18] provided a careful analysis of some of the ambiguous and previously unassigned features in the vibrational spectrum of N_4H^+/N_4D^+ for which experimental spectra have been measured,[18] using DMD with analytical potential and dipole moment surfaces.[17] Other common 57-mass protonated complexes are OC…HCO^+, N_2…HCO^+, and N_2H^+…OC. High level *ab initio* calculations have recently been carried out by several groups to characterize the structure, energetics and vibrational spectroscopic properties of OC…HCO^+ and N_2…HCO^+ complexes.[19-23] Those theoretical studies provided a detailed interpretation of vibrational spectra that place a roadmap to laboratory and interstellar detection of those species. In general, as we note below, the study of interstellar clouds requires a description of various molecular species, in neutral, positive or negative ionic or radical form to facilitate detection.[35]

The N_2H^+…OC isomer of the stable N_2…HCO^+ complex is of particular interest to computational studies due to the presence of the classic hydrogen bond.[36] Previous studies have shown[26] that N_2H^+…OC is less stable than N_2…HCO^+ by 6996 $cm.^{-1}$ Vibrational second-order perturbation theory (VPT2) calculations based on the quartic force field (QFF)[24] produced force constants, spectroscopic data, and showed that the N_2H^+…OC and N_2… HCO^+ isomers can be distinguished by the IR spectroscopy. The PES used in the QFF calculations was generated in the vicinity of the minimum energy stationary point on a grid at the CCSD(T)/aug-cc-pVXZ (X=T,Q,5) levels of theory and energies were extrapolated to the complete basis set limit with core correlation and relativistic inclusions (CcCR).[24] The spectral intensities were calculated using a double harmonic approximation with the MP2 dipole. Moreover, the dynamics of proton transfer and proton isomerization processes in the N_2 + HOC^+ reaction have been studied on the full-

dimensional global potential energy surface, computed at the CCSD(T)-F12a/aug-cc-pVTZ-F12 level of theory using quasi-classical trajectories.[25] It was found, for example, that a proton transfer is involved in forming of the N_2H^+ + OC products, while the proton isomerization process results in the N_2 + HCO^+ products. The study of this multichannel reaction predicted that the N_2H^+/HCO^+ branching ratio increased with the collision energy. Understanding these reaction mechanisms helps to provide an evidence of formations of the N_2H^+…OC and N_2…HCO^+ ion-molecular complexes, gas-phase depletion, and could facilitate the investigation of the dynamical evolution of star-forming cores.[37]

Motivated by the fact that no experimental data are currently available for the hydrogen bonded isomer and that only a limited number of theoretical studies have been reported,[24-26] in the present work, we calculate and thoroughly characterize the IR spectra of the N_2H^+…OC ion-molecular complex and its deuterated isotopologue. An additional challenge arises from the lack of an analytical potential energy surface. Therefore, we employed the direct DMD approach, supported by MD simulations to describe the vibrational spectra. Furthermore, we describe an efficient method for calculating nuclear dipole derivatives exactly along the trajectory, which ensures a proper treatment of infrared activity.

2. COMPUTATIONAL METHODS

As in the previous study of N_4H^+ complex[13] we use explicitly correlated electronic structure methods, namely, the second-order Møller-Plesset (MP2-F12)[38] and coupled cluster (CCSD(T)-F12)[39,40] methods with correlation-consistent aug-cc-pVDZ (AVDZ) basis set. Addition of the diffuse functions is important for describing properties of ions, dipole moments, as well as intra- and intermolecular bonding.[41] These explicitly correlated methods were developed to be robust

and reliable tools for the prediction of molecular structure and properties with a significant saving of computational cost; they have been shown to provide a dramatic improvement of the basis set convergence toward the complete basis set (CBS).[42,43] To validate the use of the computationally less demanding AVDZ basis set in the direct trajectory propagation, we compared structural parameters, harmonic frequencies, and energetics of the N_2H^+…OC complex to the ones obtained from MP2 and CCSD(T) methods with the larger aug-cc-pVTZ (AVTZ) basis set. We also investigate the potential energy surface and dipole moment surface for the H^+ transfer motion to better understand the fluxional motion.

Our spectral analysis involved two steps: (i) standard MD simulations were carried out to generate infrared spectra; (ii) and the most prominent spectral features were then assigned using the DMD method.[44-47] In the MD simulations, the interaction potential, forces,[48,49] the dipole moment, and its derivatives (see below) were evaluated as needed at every time step, i.e. "on-the-fly", as the trajectories were propagated. We utilized the velocity-Verlet scheme[50] to integrate Hamilton's equations of motion using a shell script that interfaces the MOLPRO program[51] and a set of FORTRAN procedures. The MD trajectories for the N_2H^+…OC and N_2D^+…OC complexes were run at constant energies (NVE), corresponding to a chosen temperature (see Results for further details), and J=0 angular momentum. We ran several independent sets of trajectories, randomly sampled, for a total propagation time of 10 ps. The integration time step was 0.5 fs, which in the past gave very reliable results at the similar total energies.[13] Additional sets of higher energy trajectories compared to the typical temperatures in the interstellar medium,[35] were also generated, at 150 K and 300 K corresponding to about 20 % and 40 % of the harmonic ZPE at the N_2H^+…OC minimum, respectively. Upon collecting all the data, we used a Fourier transform of the dipole-dipole correlation functions to obtain IR spectra,

$$I(\omega) = \frac{Re}{\pi}\int_0^\infty dt\, e^{i\omega t}\,\langle \vec{\mu}_0 \cdot \vec{\mu}_t \rangle \quad (1)$$

The operation denoted by $\langle \ldots \rangle$ involves the usual Monte Carlo average of the random trajectories, as well as a time-average over the length of the trajectory itself, as was also done by us previously.[52] These classically derived spectra were scaled by a quantum mechanical intensity-correction factor, ω/[1-exp(-ω/kT)],[53] where ω is the frequency.

The details and implementation of the DMD method were described in the series of our previously published works,[44-47,52] where we considered similar hydrogen-bonded molecular complexes N_4H^+ and N_4D^+ as well as protonated water clusters.[13,54] Briefly, in DMD, an external, sinusoidal electric field in the manner of a CW laser ablation,[55] is applied to invoke an absorption at some resonant frequency, ω. The time-dependent molecular Hamiltonian in an external electric field, to the first order of an electric field perturbation ε, is

$$H(p, q, t; \omega) = H_0(p, q) + \vec{\mu}(q) \cdot \vec{\varepsilon} \sin \omega t \quad (2)$$

where H_0 is the free molecule Hamiltonian, $\vec{\mu}(q)$ is the coordinate-dependent electric dipole moment vector, and $\vec{\varepsilon}$ is the electric field vector with the fixed laboratory frame Cartesian components X, Y, Z. The modified equations of motion accounting for the field-energy term are

$$\dot{q} = \frac{p}{m} \quad (3a)$$

$$\dot{p} = -\nabla V(q) - (\nabla \vec{\mu}) \cdot \vec{\varepsilon} \sin \omega t \quad (3b)$$

where $V(q)$ is the molecular interaction potential, m are atomic masses, and p and q are the $3N$ Cartesian momenta and coordinates, respectively.

The potential and field energy gradients in Eq. 3b are computed "on-the-fly" along the trajectory. For instance, in some of our recent work,[13] the DMD simulations were carried out using analytical potential energy (PES) and dipole moment (DMS) surfaces; both the potential gradients

and dipole derivatives were readily obtained using finite difference methods in Cartesian coordinates at a negligibly small computational cost. Somewhat similarly, in the present work, the Cartesian gradient of the potential (ΔV) is sourced directly from the electronic structure method (see above); however, straightforward differentiation of the dipole's three components with respect to the nuclear Cartesian coordinates is both impractical and unnecessary. To calculate the dot product in the Eq 3b, we re-write the field energy term, which we will interchangeably call the "driving force", without the applied sin(ωt) action, as follows,

$$(\nabla\vec{\mu}) \cdot \vec{\varepsilon} = |\vec{\varepsilon}|\nabla\mu_{\hat{\varepsilon}} \tag{4}$$

where $\mu_{\hat{\varepsilon}}$ is the molecular dipole's component, now a scalar, along the unit vector $\hat{\varepsilon}$. (See Scheme S1 in Supplementary information for details.) Now, using the standard definition of the dipole as a total electronic energy's field derivative along a laboratory-frame axis (*X*, *Y* or *Z*)

$$\nabla\mu_X = \nabla\frac{\partial V}{\partial \varepsilon_X} = \frac{\partial}{\partial \varepsilon_X}\nabla V \tag{5}$$

the scalar dipole derivative in Eq. 4 may be evaluated by a central difference formula as follows,

$$\nabla\mu_{\hat{\varepsilon}} = \frac{\partial g}{\partial \lambda_{\hat{\varepsilon}}} = \lim_{\lambda \to 0}\left[\frac{g(\lambda\hat{\varepsilon}) - g(-\lambda\hat{\varepsilon})}{2\lambda}\right] \tag{6}$$

where $g \equiv \nabla V$, and λ is the value of the electric field applied along the unit vector $\hat{\varepsilon}$. Thus, we rewrite Eq. 3b as

$$\dot{p} = -g - \frac{\partial g}{\partial \lambda_{\hat{\varepsilon}}}|\vec{\varepsilon}| \sin\omega t \tag{7}$$

with the numerical approximation

$$\frac{\partial g}{\partial \lambda_{\hat{\varepsilon}}} \approx \frac{g(\lambda\hat{\varepsilon}) - g(-\lambda\hat{\varepsilon})}{2\lambda} \tag{8}$$

using an arbitrarily small value of λ, e.g. 0.0005-0.001 a.u. The quantity in Eq. 8. depends on the molecule's orientation (through its dipole vector) with respect to the electric field, whose direction is fixed during a trajectory. Thus, there is a torque applied to the molecular frame, and the total

angular momentum in the DMD trajectory is generally not conserved, except in certain symmetry restricted cases.

In summary, to update the momenta, three gradients are evaluated (i) g, the gradient with zero field, (ii) $g(\lambda\hat{\varepsilon})$, the gradient with a field of value λ applied in $\hat{\varepsilon}$ direction, and (iii) $g(-\lambda\hat{\varepsilon})$, the gradient with a field of value λ applied in $-\hat{\varepsilon}$ direction. Therefore, the computational effort of a DMD trajectory is three times that of a conventional trajectory. We note that $g(\pm\lambda\hat{\varepsilon})$ may be computed at a lower level of theory than g, since Eq. 8 does not depend on the latter, making it possible to devise various computationally less expensive approaches, as has been done in the past,[56-58] without a significant sacrifice in accuracy. Also, in our previous study of N_4H^+,[13] we used the analytical potential that was calculated at the CCSD(T)-F12b/AVTZ level of theory, while the dipole moment surfaces were evaluated at the lower level, MP2/AVTZ.

In this work, we use the MP2-F12/AVDZ level of theory to evaluate the PES and its gradient and the MP2/AVDZ level of theory to calculate the driving force in DMD. IR active vibrations in the MD spectra were analyzed by running the DMD simulations up to 3 ps, with a 0.5 fs time step in the range of frequencies from 40 to 2700 cm^{-1}, and with a frequency step of 20 cm^{-1} in the regions where significant absorptions occur and at all harmonic frequencies. A total of 200 trajectories were propagated for N_2H^+…OC and N_2D^+…OC to obtain the DMD spectrum. Additional trajectories were run at the higher level of theory, CCSD(T)-F12/AVDZ to obtain the MD spectrum and reevaluate some key features using the CCSD(T)/AVDZ driving force.

The average absorbed internal energy at a driven frequency ω is defined as

$$\langle H_0(\omega)\rangle = (1/t)\int_0^t H_0(t',\omega)\,dt'. \qquad (9)$$

The atomic coordinates, dipoles, dipole derivatives, forces, and total energies are collected along each trajectory for rigorous analysis.

To aid the assignment of spectral features, non-harmonic fundamental frequencies, overtones, and combination bands were calculated variationally using the VSCF[59] and VCI[60,61] methods. The VCI calculations included three-mode coupling of the potential energy and dipole surfaces. The basis for the VCI calculations consisted of all VSCF product wave functions up to quintuple excitations within a single mode, with simultaneous excitations up to the quadruple level (VCISDTQ), and with the added restriction of a maximum sum of 10 quanta. All electronic structure calculations, normal mode analysis, and VSCF/VCI calculations were performed using the MOLPRO 2019 software package.[51]

3. RESULTS AND DISCUSSION

(a) Normal mode analysis and MD simulations

It was previously reported that the minimum structure of the N_2H^+…OC complex is linear.[26] Our calculations similarly show the global minimum on the potential energy surface to be of $C_{\infty v}$ symmetry, and we also confirmed the existence of a T-shaped transition state (C_s symmetry) for the CO rotation. This transition state describes CO rotation around N_2H^+ to yield the more stable isomer, N_2… HCO^+.[25] The structural parameters, dipole moments, and harmonic frequencies for the global minimum and TS are collected in the Supplemental information (**Tables S1-S3)**. The MP2-F12/AVDZ and CCSD(T)-F12/AVDZ structural parameters agree within 0.01 Å with the MP2/AVTZ and CCSD(T)/AVTZ values. The dissociation energy for fragmentation of N_2H^+…OC into N_2H^+ and CO is rather sensitive to the level of theory (**Table S4)**. The CCSD(T)/AVTZ dissociation energy D_e and its harmonic zero-point corrected value D_o were estimated to be 4997 cm^{-1} (14.3 kcal/mol) and 4810 cm^{-1} (13.8 kcal/mol), respectively. **Figure 1** shows that there is a negative electrostatic potential (ESP) at the CO bond for both the minimum and T-shaped transition state. The values of the dissociation energy for the process N_2H^+…OC →

N_2H^+ + CO and the T-shape barrier height of 3728 cm^{-1} (10.7 kcal/mol) at the CCSD(T)/AVTZ level of theory for the CO rotation provide a clear indication that N_2H^+…OC is long-lived enough to be observable at the low temperatures. N_2H^+…OC has a large dipole moment of 0.808 a.u. (2.05 D) at the CCSD(T)/AVTZ level of theory[26] which can support its detection using infrared spectroscopy. For comparison, the dipole moment of the water molecule is 0.727 a.u. (1.85 D).[62]

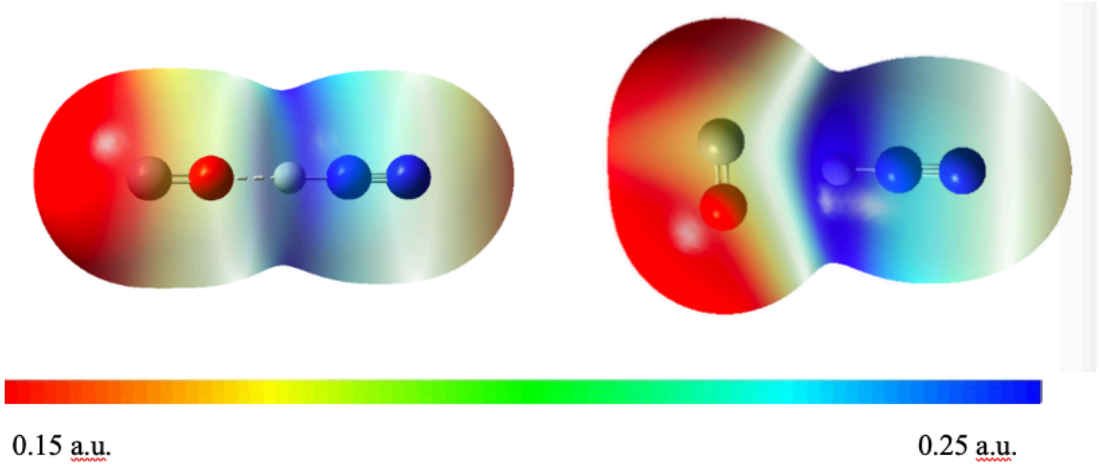

Figure 1. Electrostatic potential maps at the MP2/AVTZ level of theory (density isovalues = 0.0004 a.u.) for the equilibrium structure and T-shaped transition state of N_2H^+…OC generated using the Gaussview program.[63]

Tables 1-2 summarize vibrational frequencies obtained from our MD and DMD simulations, our VSCF/VCI, and previous VPT2 calculations.[24] At first, MD MP2-F12/AVDZ spectra were obtained at internal energies ranging from 31 cm^{-1} to 1877 cm^{-1} corresponding to temperatures from 5 K to 300 K (**Figures 2a-2e**). The vibrational spectrum at low temperature (**Figure 2a**) closely resembles the harmonic "normal mode" spectrum. There we can identify the two lowest frequencies at 96 cm^{-1} and 192 cm^{-1} which can be confidently assigned to the bending (π symmetry) modes involving the CO and NN moieties, and the one at 265 cm^{-1} to the CO…NN σ stretch intramolecular vibration. There are additional peaks, provisionally interpreted as

overtones and combination bands in the low frequency range at 240, 380 and 450 cm^{-1} that are clearly visible only at the higher energy MD simulations **(Figure 2e**).

Table 1: Anharmonic Frequencies (in cm^{-1}) of CO…HNN^+. ($C_{\infty v}$ symmetry)

	VSCF MP2-F12	VCI MP2-F12[b]	MD MP2-F12	DMD MP2-F12[a]	MD CCSD(T)-F12	VPT2[c] CcCR
ν_1 (σ)	2226	2234	2425	2380	2600	2394.0
ν_2 (σ)	2001	2019	2020	2040	2080	2073.9
ν_3 (σ)	1762	1541	1800	1800	1785	1620.4
ν_4 (π)	969	954	910	910	925	1280.7
ν_5 (σ)	281	294	230	240	245	286.7
ν_6 (π)	231	202	190	192	195	282.7
ν_7 (π)	157	114	90	96	90	156.5
$2\nu_4$	1938	1902	1970	1980	1985	2761.0
$\nu_5+\nu_6$	512	505	450	450	465	581.0
$\nu_5+\nu_7$	438	421	380	380	385	456.8
$\nu_6+\nu_7$	388	356/367				450.2
$\nu_4+\nu_7$	1126	1085/1096/1090		980	1010	1479.7

[a]The field strength in the DMD simulations was 75 mV/bohr. Weaker absorptions at 380 and 450 cm^{-1} modes were excited only by the stronger field of intensity 150 and 200 mV/bohr, respectively. [b] Mode mixing was observed in some cases. [c]Reference 24.

Table 2: Anharmonic Frequencies (in cm^{-1}) of CO…DNN^+. ($C_{\infty v}$ symmetry)

	VSCF MP2-F12	VCI MP2-F12[b]	MD MP2-F12	DMD MP2-F12[a]	MD CCSD(T)-F12	VPT2[c] CcCR
ν_1 (σ)	2255	2212	2325	2300	2480	2407.4
ν_2 (σ)	1995	2014	2035	2010	2030	2057.1
ν_3 (σ)	1271	1211	1330	1360	1300	1214.7
ν_4 (π)	717	712	680	680	700	894.2
ν_5 (σ)	270	261	230	240	230	275.7
ν_6 (π)	226	195	185	180	185	266.5
ν_7 (π)	157	110	90	95	100	144.2
$2\nu_4$	1434	1415	1500	1460	1500	1946.1
$\nu_5+\nu_6$	496	481	460		460	556.6
$\nu_5+\nu_7$	427	402	370	370	375	436.3
$\nu_6+\nu_7$	383	341/354				421.4

[a]The field strength in the DMD simulations was 75 mV/bohr. [b] Mode mixing was observed in some cases. [c]Reference 24.

A notable doublet near 1929 cm^{-1}, seen in **Figure 2a**, is missing in the normal mode spectrum, where only one peak shows up at this frequency. This 1929 cm^{-1} harmonic fundamental mode corresponds to the parallel proton stretch vibration (see **Table 1**). It becomes split as MD simulations are run at progressively higher energies (**Figures 2a-2e**). Moving away from the harmonic limit to the stronger inter-mode coupling regime, the doublet splits into two separate peaks, the weaker one at 1800 cm^{-1} and the stronger one at 1970 cm^{-1}. Based on the overtone analysis of the harmonic spectrum, and DMD simulations in this energy range (see below), we provisionally speculate that the companion peak in the low-energy MD spectrum doublet arises from a Fermi-like resonance between a parallel proton motion and perpendicular proton bending overtone, i.e. the formally dark harmonic π^2 overtone with the 2×956 cm^{-1} transition frequency, (see **Table 1S)**. As the MD energy increases, the modes interact via the cubic, quartic, and higher order terms and move away from a resonance regime while the intensity of the overtone peak decreases rather noticeably. In our previously reported $H_5O_2^+$ MD simulations, we also observed similar classical Fermi resonances involving the shared proton motion.[44,54] The low intensity peak in the N_2H^+ …OC spectrum at 2050 cm^{-1} can be ascribed to the CO stretch vibration.

The high energy MD spectra for N_2H^+…OC and its deuterium isotopologue were also calculated at the MP2-F12/AVDZ level of theory and compared to the CCSD(T)-F12/AVDZ results (**Figure 3**). MD CCSD(T)-F12/AVDZ spectra show a doublet with the maxima at 1785/1985 cm^{-1} and 1275/1500 cm^{-1}, for N_2H^+…OC and N_2D^+…OC, respectively. The corresponding simulations at the MP2-F12/AVDZ level of theory show the doublet at 1800/1970 cm^{-1} and 1330/1500 cm^{-1}, respectively. A comparison of the MP2-F12 and CCSD(T)-F12 results is suggesting that the doublet is not an artifact of the lower level electronic structure method, MP2-F12/AVDZ (**Figures 2a-2e**). Also, in the supplementary information, we show that the DMD

MP2-F12/AVDZ and CCSD(T)-F12/AVDZ simulations produce very similar absorption profiles and internal coordinate excitation signatures for the parallel H^+ stretch vibration (Figure 1S). These findings rationalize running the extremely time-consuming DMD scans at the lower level of theory, MP2-F12/AVDZ, to assign the vibrational spectra.

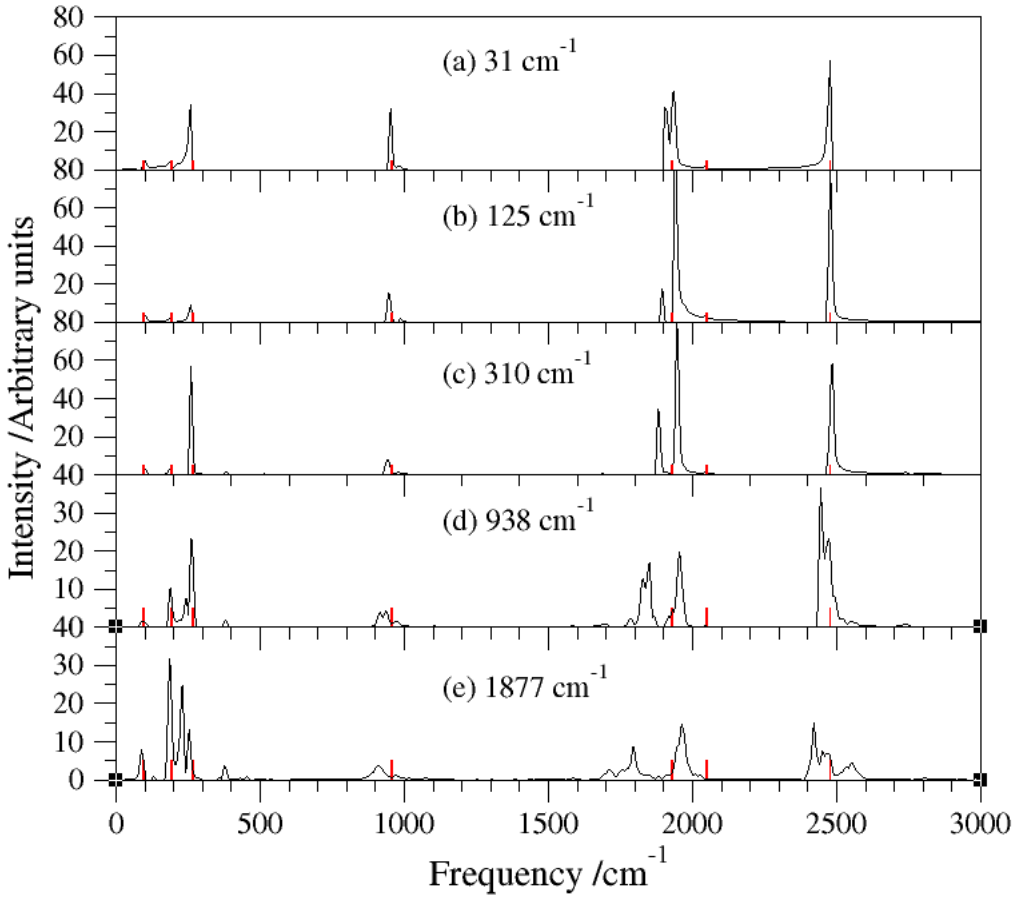

Figure 2. NVE equilibrium MD MP2-F12/AVDZ dipole spectra of N_2H^+ …OC propagated at total energies ranging from 31 cm^{-1} to 1877 cm^{-1}. The harmonic frequencies are shown as red sticks.

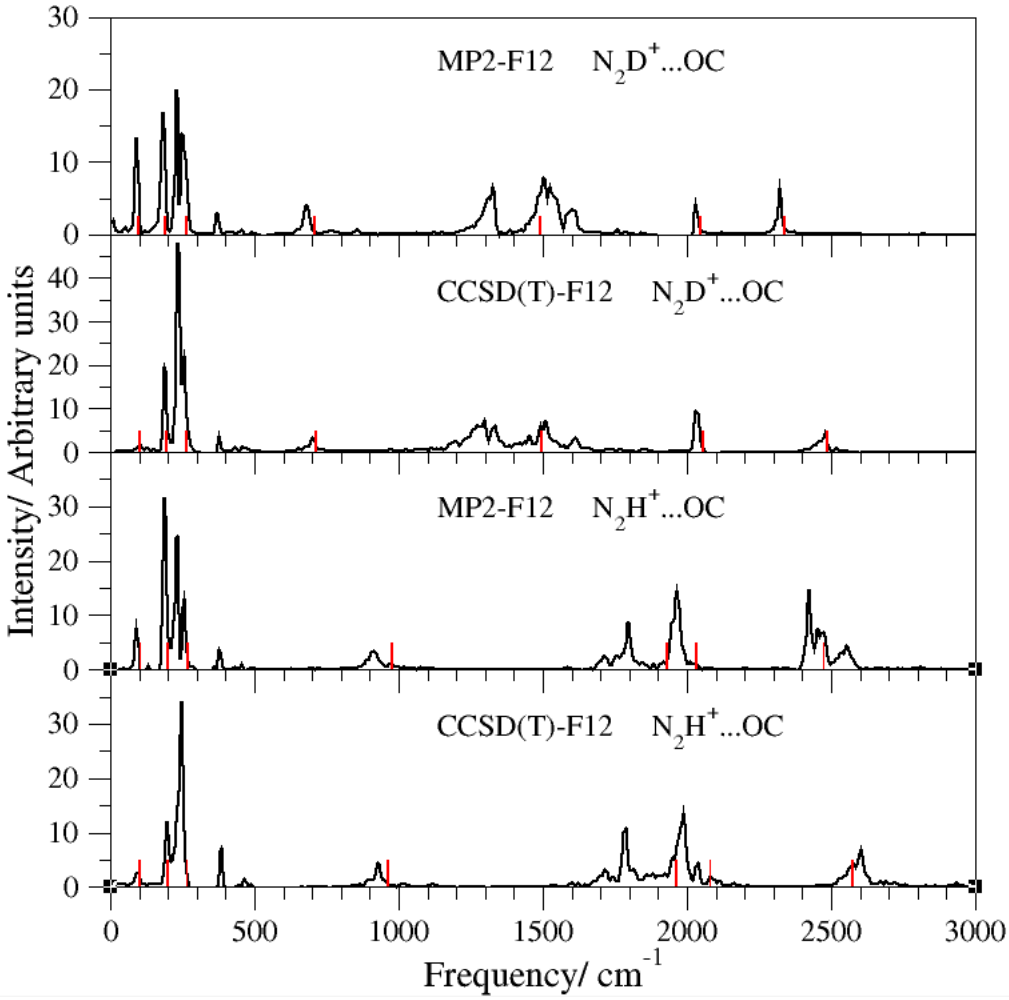

Figure 3. NVE direct equilibrium MD MP2-F12/AVDZ and CCSD(T)-F12/AVDZ dipole spectra of N_2H^+ …OC and N_2D^+…OC propagated at the total energy of 1877 cm^{-1}. The harmonic frequencies are shown as red sticks.

To facilitate discussion, we find it useful to perform VSCF/VCI calculations at the MP2-F12/AVDZ level of the theory to assess anharmonic effects in vibrational spectra. Three dimensional potential energy surface cuts were generated around the minimum, and a three mode coupling scheme was used in the VCI calculations. The VSCF/VCI fundamental frequencies, overtones, and combination bands for N_2H^+…OC and N_2D^+…OC are collected in **Tables 1-2** and **Table S5.**

N_2H^+…OC vibrations involving a light H^+ proton are the parallel stretch (ν_3), perpendicular H^+ bending (ν_4), and NN/NH stretch (ν_1). As noted in the earlier work, in the centrosymmetric linear complex N_4H^+, the H^+ parallel stretch showed very large anharmonic shifts.[13-18] The CCSD(T)-F12b/AVTZ harmonic frequency is 93 cm^{-1}, while highly accurate quantum VCI calculations[17] studies predicted the H^+ stretch at 759 cm^{-1}, and the corresponding experimental observation[18] was at 743 cm^{-1}. In the asymmetric linear complex, N_2H^+…OC, VPT2 calculations based on the quartic force fields (QFF) by Fortenberry et. al also showed a large anharmonic shift[24] for the H^+ parallel stretch. Their reported harmonic and anharmonic values were 1976.6 and 1620.4 cm^{-1}, respectively. The QFF method uses the fourth-order Taylor series approximation to describe the PES near the equilibrium.[64] Then rovibrational spectra are determined using the vibrational perturbation theory (VPT2). We compared the H^+ motion in the N_2H^+…OC complex to the one in the N_4H^+ complex. We carried out the relaxed scans at the CCSD(T)-F12/AVDZ level of theory along the N–H stretch normal mode coordinate (**Figure 4a)**. Both potential energy curves for N_4H^+ and N_2H^+…OC are relatively broad and barrierless i.e. the potentials are dominated by the cubic and higher order terms. Therefore, large anharmonic shifts were predicted for the H^+ motion. We note that in N_2H^+… OC, the H^+ is bound tightly within the N_2H^+ moiety. For example, the respective equilibrium N-H interatomic distances are 1.1085 Å and 1.2785 Å (a difference of 0.17

Å) in N_2H^+…OC and N_4H^+. Thus, as H^+ moves away from N towards O, forming the weaker bond, the potential is strongly asymmetric.

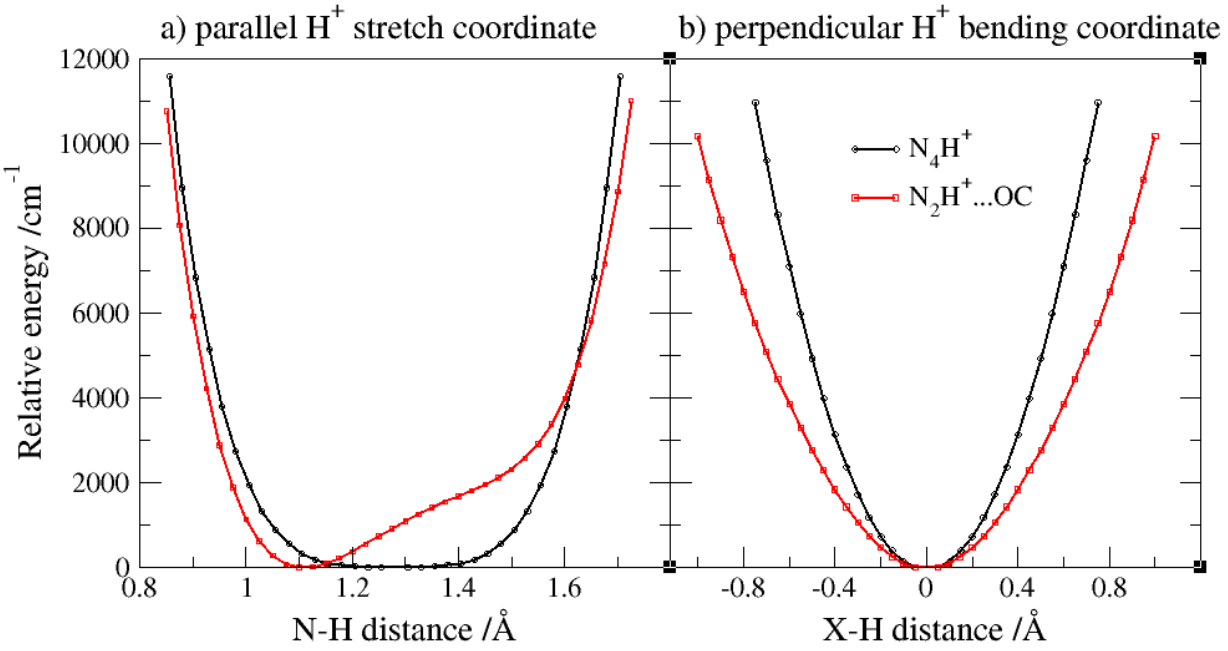

Figure 4. CCSD(T)-F12/AVDZ relaxed scan along the a) parallel H^+ stretch and b) perpendicular H^+ bending coordinates. The energies are shown relative to minimum structures. For the parallel H^+ stretch coordinate, these curves were fitted to the 6th order polynomial of displacement coordinate, $x=R(N–H) - R_e$: $\Delta E = –1.2084 – 0.014461\, x + 1872.7\, x^2 – 4.4824\, x^3 + 291110\, x^4 – 6.8242\, x^5 + 2952800\, x^6$ for N_4H^+, $\Delta E = 1.278 + 4.5054\, x + 64932\, x^2 – 246890\, x^3 + 380920\, x^4 – 315070\, x^5 + 3.13540\, x^6$ for N_2H^+…OC, respectively. For the perpendicular H^+ bending coordinate, the displacement coordinate was defined as $x=R$(X-H), where X is the center of mass of the four heavy atoms. The corresponding 6th order polynomial of displacement coordinates are $\Delta E = -54.086 + 19651\, x^2 + 2059.7\, x^4 – 3835.6\, x^6$ for N_4H^+ and $\Delta E = –15.213 + 12231\, x^2 – 5242.7\, x^4 + 3233.4\, x^6$ for N_2H^+…OC, respectively.

The present calculations are in apparent disagreement with the VPT2 calculations[24] in terms of the H^+ and D^+ bending fundamentals, previously reported at 1280.7 cm^{-1} and 894.2 cm^{-1}, respectively. Fortenberry et al. predicted a strong positive anharmonicity for the perpendicular H^+

bending mode (ν_4). The high level quantum calculations for the similar N_4H^+ complex predicted a relatively small negative anharmonic shift for the perpendicular H^+ bending mode, on the other hand.[17] For a clearer perspective, we plot N_4H^+ and N_2H^+…OC 1-D relaxed potentials along the proton bending normal mode (**Figure 4b**). We fit the potentials to a polynomial with respect to the displacement coordinate and see that the quadratic terms dominate, while all the higher order terms are much smaller. Our MD CCSD(T)-F12/AVDZ spectra for N_2H^+…OC and N_2D^+…OC (**Figure 3**) show IR activity at 925 cm^{-1} and 700 cm^{-1}, respectively. The corresponding CCSD(T)-F12/AVDZ harmonic values 962 cm^{-1} and 711 cm^{-1} (Tables 1S-2S) indicate that the anharmonicities are relatively small for the perpendicular proton bending mode, consistent with the potential energy curve analysis (**Figure 4b**).

We also analyzed molecular dipoles along the H^+ stretch (**Figure 5a**) and H^+ bending coordinates (**Figures 5b-5c**). In all cases the dipole moment components exhibit strong non-linearity. Especially notable is the dominance of quadratic terms in the z-component of the dipole moment along the coordinate describing H^+ motion perpendicularly in respect to a molecular axis. Presence of quadratic powers in the dipole, it can be argued, should result in at least some IR activity of overtone bands, which is obviously the case for the quantum harmonic oscillator. Also, the non-linear dipole plots explain the strong mixing of the low frequency modes into the proton transfer frequency range, as will be discussed below.

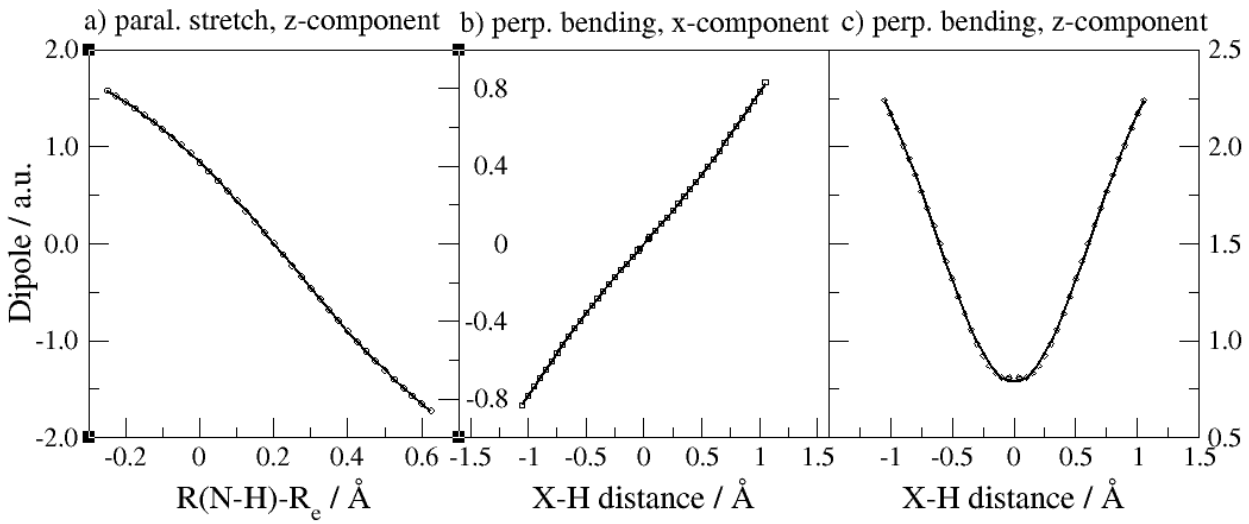

Figure 5. Dipole moment components (in atomic units) as a function of displacement for N_2H^+…OC obtained from the CCSD(T)-F12/AVDZ relaxed scans. The molecule axis is along the z-axis. X is the center of mass of the four heavy atoms. All curves were fitted to the 6th order polynomial of displacement coordinate, *x*.

a) $\mu = 0.84172 - 3.6957\,x - 2.9498\,x^2 + 1.3009\,x^3 + 5.5632\,x^4 - 0.084926\,x^5 - 4.4301\,x^6$

b) $\mu = 0.6816\,x + 0.13885\,x^3 - 0.036275\,x^5$

c) $\mu = 0.78618 + 2.451\,x^2 - 1.4834\,x^4 + 0.41392\,x^6$

(b) DMD simulations

Moderate energy absorption rate was observed with the applied field strength of 75 mV/bohr (**Figure 6**), while a stronger field was occasionally used to induce absorption at less active frequencies. Red sticks in the DMD scan pinpoint the harmonic frequencies and imply anharmonic shifts for some modes, and additional anharmonic features. More interestingly, DMD scans reveal very broad spectral features where the doublets at 1800/1980 cm^{-1} (1360/1460 cm^{-1}) in the MD MP2-F12/AVDZ spectra were predicted for N_2H^+…OC (N_2D^+…OC), respectively. Also, there is broad spectral feature near the perpendicular H^+ bending fundamental in N_2H^+…OC.

Prominent spectral features of N_2H^+…OC and N_2D^+…OC were assigned by inspecting the atomic motion and analyzing the driving force, as well as by VCI calculations. **Figures 7-9** and in the additional figures in the Supplemental information (**Figures 1S-4S)** depict the average

absorbed energy and the key internal coordinates as functions of time. **Figure 7** shows the analysis of the DMD trajectory driven at the frequency ν_1=2380 cm^{-1}. There, average absorbed internal energy $\langle H_0(\omega)\rangle$ increases rapidly, in a quasi-exponential curve; then it executes oscillations as dephasing sets in. Large NN and NH displacements and bond angle values near 180 degrees indicate the σ character of this vibration, assigned to the NN/NH stretch. The corresponding harmonic frequency at MP2-F12/AVDZ level of theory is 2477 cm^{-1}, while both MD and DMD simulations show a broad spectral feature in the range from 2380 to 2600 cm^{-1}. The previously reported VPT2 value[24] for the NN/NH stretch is 2394.0 cm^{-1}.

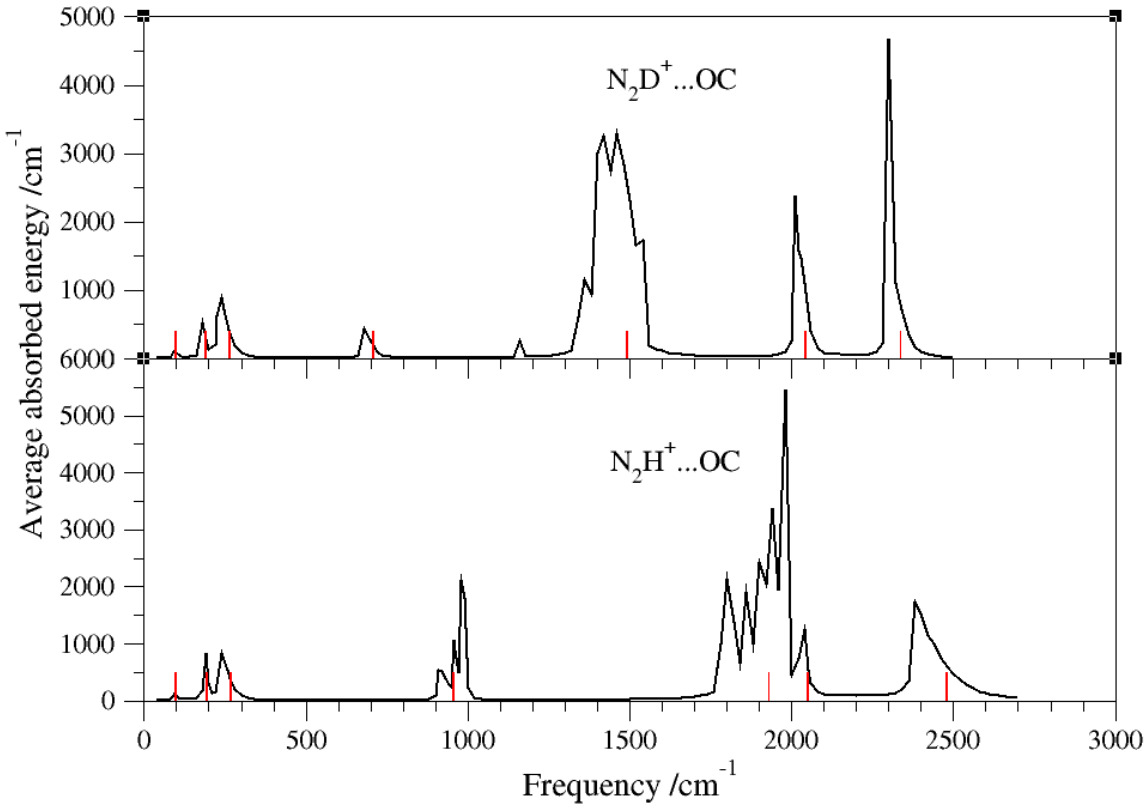

Figure 6. DMD MP2-F12/AVDZ simulations: the average absorbed energy of N_2H^+ …OC and N_2D^+…OC is plotted as a function of the driven frequency. The spectrum was scanned with a frequency step of 20 cm^{-1}. The intensity of the electric field was 75 mV/bohr. The harmonic frequencies are shown as red sticks.

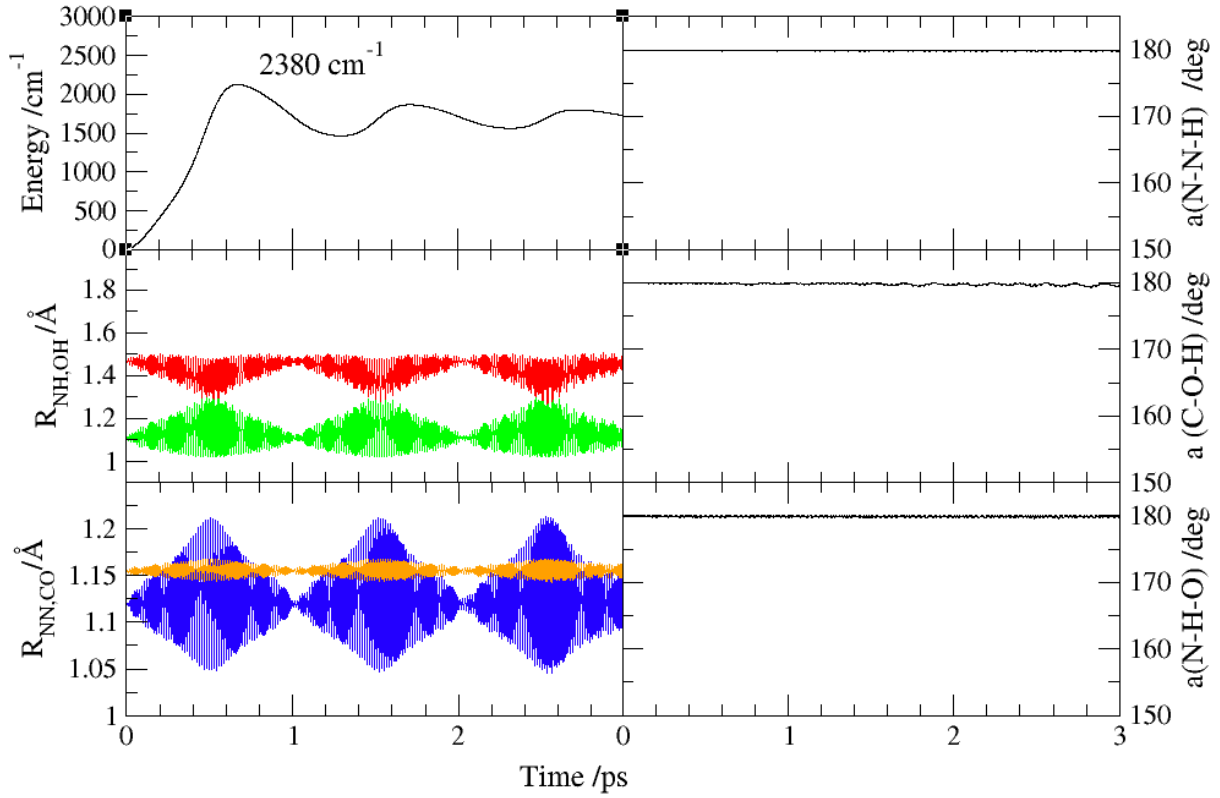

Figure 7. DMD MP2-F12/AVDZ analysis for the N_2H^+ …OC fundamental frequency ν_1=2380 cm^{-1}. Average absorbed energy is in cm^{-1}, interatomic distances are in Å (OH in red, NH in green, CO in orange, and NN in blue), and bond angles are in degrees. The intensity of the electric field was 75 mV/bohr.

The H^+ parallel stretch mode is strongly anharmonic, as is evident from the potential energy curve, fitted by a polynomial **(Figure 4a)**. The previous VPT2 theoretical studies[24] predicted its fundamental transition at 1620.4 cm^{-1}. **Figure 8** compares energy profiles and coordinates for two driven frequencies 1800 cm^{-1} and 1980 cm^{-1} corresponding to the doublet in the MD spectrum of N_2H^+…OC. The lower frequency trajectory shows a stronger H^+ parallel stretch activity, while the upper frequency shows more bending character. An extended DMD scan with the electric field strength of 75 mV/bohr (**Figure 6**) shows activity at the frequencies as low as 1700 cm^{-1}. Based on our VCI calculations (**Table 1**), we assigned the 1800 cm^{-1} transition to the parallel H^+ stretch fundamental,ν_3 and the 1980 cm^{-1} one to an H^+ bending overtone, $2\nu_4$. The corresponding VCI

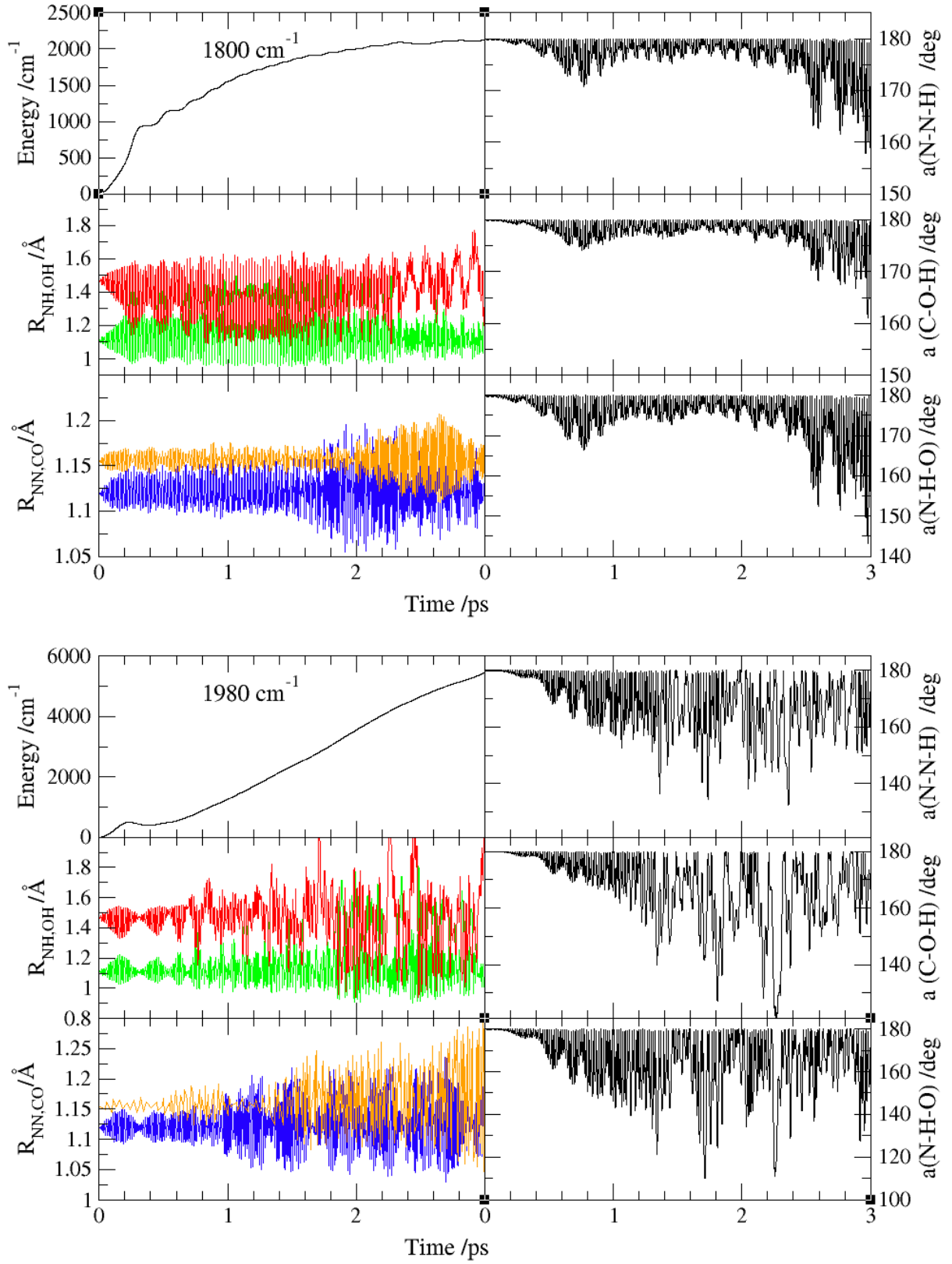

Figure 8. DMD MP2-F12/AVDZ analysis for the N_2H^+ …OC fundamental frequency ν_3=1800 cm^{-1} and overtone $2\nu_4$=1980 cm^{-1}.

values for H^+ parallel stretch and $2\nu_4$ overtone are 1541 cm^{-1} and 1902 cm^{-1}, respectively. This information is useful in the sense that the same trend can be observed for the 1360/1460 cm^{-1} doublet in the deuterium substituted isotopologue, $N_2D^{+}\cdots OC$ **(Figure 2S** in the supplemental information). The analysis of the DMD trajectories at 1360 cm^{-1} shows that OD/ND displacements are large for the D^+ parallel stretch motion, ν_3. The OD/ND out-of-phase oscillations continue periodically up to 1.5 ps, while the bond angle oscillations are relatively small. For the 1460 cm^{-1} mode assigned to D^+ bending overtone, $2\nu_4$, the OD/ND distances increase significantly from the early start of trajectory. Also, we note very large bond and angle displacements that are visible along the trajectory. The corresponding D^+ parallel stretch at the VCI level of theory is 1211 cm^{-1} is in very good agreement with the VPT2 value[24] of 1212 $cm.^{-1}$

Our DMD calculations show a very intense peak at 980 cm^{-1} and a weaker, satellite feature at 910 cm^{-1} (**Figure 6**). We note, and the evidence is provided in SI (**Figure 3S**) that the perpendicular proton motion for the deuterium isotopologue is at 680 cm^{-1} (corresponding harmonic frequency is 707 cm^{-1}). The $N_2H^+\ldots OC$ trajectory driven at 910 cm^{-1} and the one for the corresponding deuterium isotopologue at 680 cm^{-1} exhibit similar profiles. The average absorbed energies increased up to 700 cm^{-1} (87 meV), then decreased slightly, indicating a quick onset of dephasing at this frequency. Bond angle deviations are very large, interatomic distance changes are relatively small and exhibit periodicity. Based on the above observations, these modes were assigned to the perpendicular proton bending fundamental vibration (ν_4).

A DMD trajectory of N_2H^+...OC driven at 980 cm^{-1} mode absorbed rapidly (**Figure 9**) compared to the weaker absorption at 910 cm^{-1} fundamental frequency. Strong energy absorption at 980 cm^{-1} resulted in large displacements of all interatomic distances and bond angles. This frequency is tentatively assigned to a combination band of $\nu_4 + \nu_7$ (the perpendicular proton

bending and low frequency bending) because of correlated changes in NH and OH interatomic distances and bond angles as seen in **Figure 9**. This finding is supported by the non-linearity of the dipole moment (**Figures 5b-5c**) and highly oscillatory nature of the driving force along the resonant frequency (**Figures 10**).

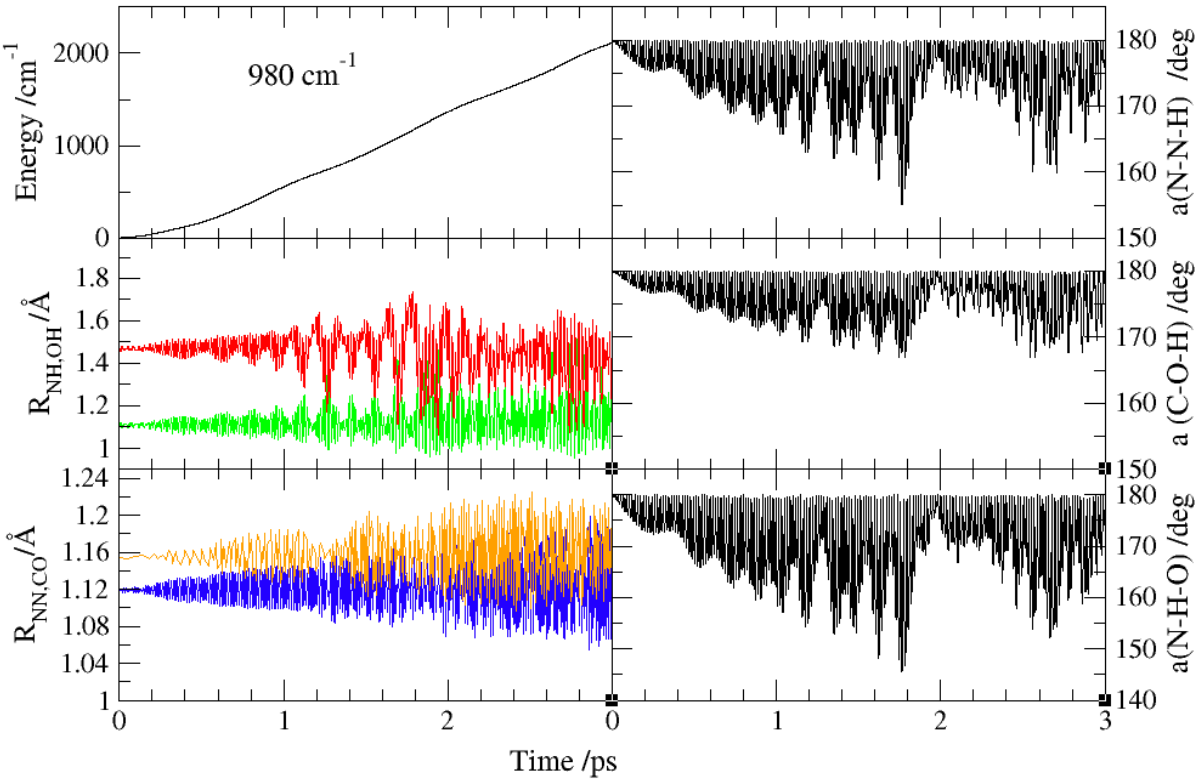

Figure 9. DMD MP2-F12/AVDZ analysis for the N_2H^+…OC combination band $\nu_4+\nu_7$=980 cm^{-1}.

The weak activity was seen in the high energy MD-MP2-F12/AVDZ spectra at 380 cm^{-1} and 450 cm^{-1} (**Figure 3**). These modes were recovered by DMD using a hard driving regime with a stronger electric field of 150-200 mV/bohr and a longer propagation time up to 5-10 ps (**Figure 4S).** The trajectory driven at 380 cm^{-1} did not absorbed energy up to 2 ps, executing only small atomic displacements. After 2 ps, energy was absorbed moderately. This time delay was also observed in combination bands of the N_4H^+ complex[13] as well as water clusters.[4,54] Small NH and

large OH displacements in N_2H^+…OC are attributed to the NN…OC parallel stretch (ν_5) motion and angular displacements to low bending modes, ν_6 and ν_7. 380 and 450 cm^{-1} modes were assigned to combination bands of the low frequency bending and stretching modes $\nu_5+\nu_7$ and $\nu_5+\nu_6$, respectively. The supporting evidence can be seen in the VCI calculations (**Table 1**).

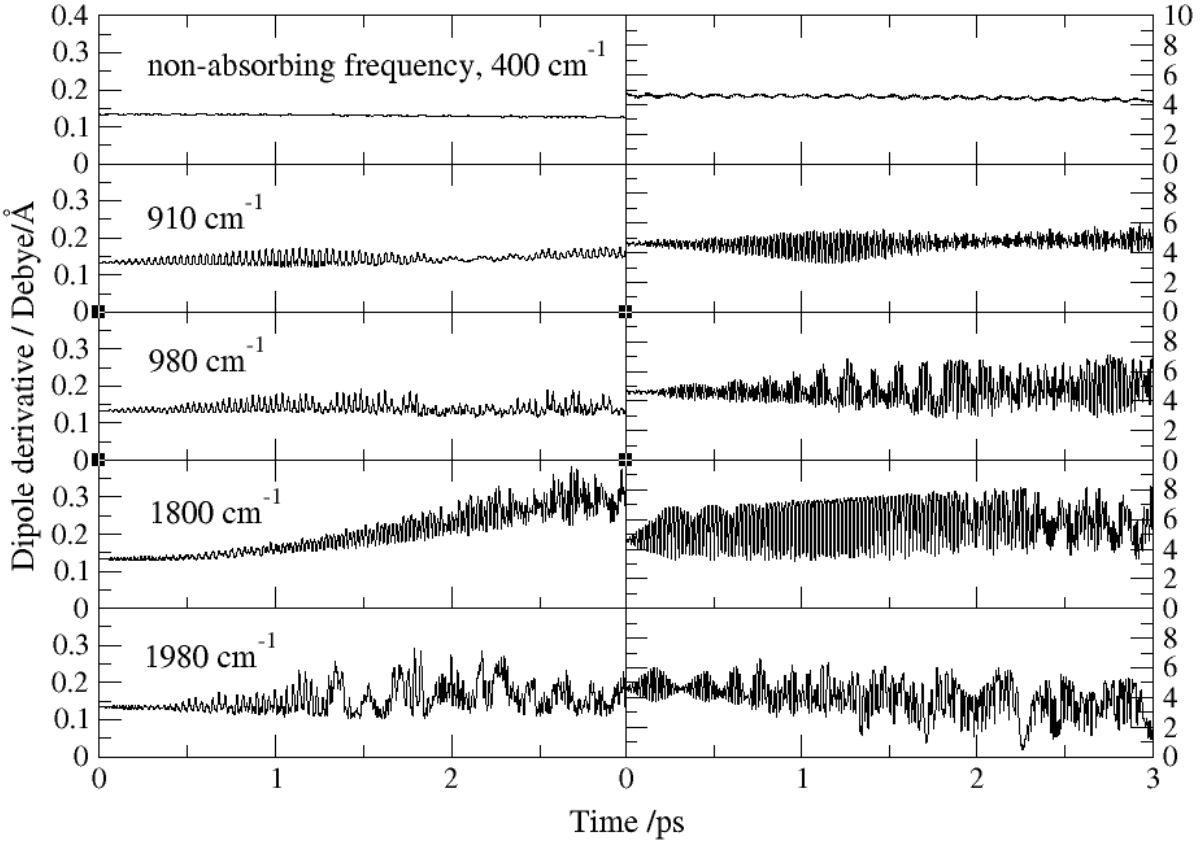

Figure 10. The driving force (Eq. 4) was monitored for frequencies involving H^+ motion in the perpendicular (left panel) and parallel (right panel) direction with respect to the molecular axis. For comparison, the driving force for non-absorbing (inactive frequency) is also shown.

4. SUMMARY AND CONCLUDING REMARKS

In the present work, the IR spectra of N_2H^+…OC and its deuterium isotopologue were characterized using classical MD simulations at the MP2-F12/AVDZ and CCSD(T)-F12/AVDZ levels of theory. The electric field driven classical trajectories were carried out at the MP2-F12/AVDZ level of theory for the potential energy and MP2/AVDZ for the dipole moment. The following key findings are reported:

(i) The vibrational modes involving H^+ and D^+ were predicted in the mid-IR range [900, 2600] cm^{-1} and [700, 2500] cm^{-1}, respectively.

(ii) The MD CCSD(T)-F12/AVDZ simulations suggest Fermi-like resonance doublets 1785/1985 cm^{-1} and 1275/1500 cm^{-1}, in the region of the shared proton stretch of N_2H^+…OC and N_2D^+..OC, respectively, resulting from the interaction of the parallel proton stretch and perpendicular proton bending overtone.

(iii) Classical trajectory simulations could be overestimating the proton fundamental stretch due to the strong non-harmonicity of the PES. Our quantum variational VCI calculations predict the H^+ stretch vibration as low as 1541 cm^{-1}. We have not observed large positive anharmonicity for the perpendicular H^+ bending vibration as predicted in a previous work by Fortenberry et al.[24] We have predicted it at 925 cm^{-1} in the MD CCSD(T)-F12/AVDZ spectrum and the corresponding harmonic values was 962 $cm.^{-1}$ Such a small anharmonic shift[13] was also observed in the N_4H^+ complex, where the H^+ bending vibration is much more harmonic.

(iv) The DMD MP2-F12/AVDZ calculations driven at 980 cm^{-1} reveal a strong mode mixing of perpendicular proton bending and low frequency bending modes. Weak absorptions at 380 cm^{-1}

and 450 cm^{-1} were ascribed to combination bands of the low frequency bending and stretching modes.

(v) Finally, we note that the herein described method of evaluating the field-dipole energy gradient, i.e. the driving force, is highly encouraging for more complex applications of the "on-the-fly" DMD method, such as 2D-IR simulations of biologically relevant systems, where analytical PES/DMS are not available. These simulations are presently being explored.

This analysis supports the previous theoretical studies aimed at detection of the N_2H^+…OC in the interstellar clouds as well as analysis of the interesting hydrogen-bonded complex.

ACKNOWLEDGEMENTS

This work was supported by the National Science Foundation (Grant No. CHE–1855583). We thank Advanced Computer Services at Kennesaw State University for providing a high-performance computing platform.

Notes

The authors declare no competing financial interests.

ASSOCIATED CONTENT

Supporting Information. The Supporting Information is available free of charge on the ACS Publications website. This contains structural parameters, harmonic vibrational frequencies, VCI overtones and combination bands, and details of driven molecular dynamics analysis.

AUTHOR INFORMATION

Corresponding Author
*Email: mkaledin@kennesaw.edu (M.K.), ORCID 0000-0003-1763-3552

REFERENCES

(1) Zundel, G. In the Hydrogen Bond: Recent Developments in Theory and Experiment. Schuster, P., Zundel, G.; Sandorfy, C., Eds.; North-Holland: Amsterdam, **1976**; Vol. 2, p 683.

(2) Giguere, P. A.; Turrel, S. The Nature of Hydrofluoric Acid. A Spectroscopic Study of the Proton-Transfer Complex $H_3O^+.F^-$. *J. Am. Chem. Soc.,* **1980**, *102*, 5473-5477.

(3) Librovich, N. B.; Sakun, V. P.; Sokolov, N. D. H^+ and OH^- Ions in Aqueous Solutions Vibrational Spectra of Hydrates. *Chem. Phys.,* **1979**, *39*, 351-366.

(4) Esser, T. K.; Knorke, H.; Asmis, K. R.; Schollkopf, W.; Yu, Q.; Qu, C.; Bowman, J. M.; Kaledin, M. Deconstructing Prominent Bands in the Terahertz Spectra of $H_7O_3^+$ and $H_9O_4^+$: Intermolecular modes in Eigen Clusters. *J. Phys. Chem. Lett*., **2018**, *9*, 798-803.

(5) Kaledin M.; Kaledin, A. L.; Bowman, J. M. Vibrational Analysis of the $H_5O_2^+$ Infrared Spectrum Using Molecular and Driven Molecular Dynamics. *J. Phys. Chem. A*, **2006**, *110,* 2933-2939.

(6) Huang, X. C.; Cho, H. M.; Carter, S.; Ojamae, L.; Bowman, J. M., Singer, S. J. Full-dimensional Quantum Calculations of Vibrational Energies of $H_5O_2^+$. *J. Phys. Chem. A,* **2003**, *107*, 7142- 7151.

(7) McCoy, A.B.; Huang, X. C.; Carter, S.; Landerweer, M. Y.; Bowman, J. M. Full-dimensional Vibrational Calculations for $H_5O_2^+$ Using an *ab initio* Potential Energy Surface. *J. Chem. Phys.,* **2005**, *122*, 061101.

(8) White, E. T.; Tang, J.; Oka, T. CH_5^+: The Infrared Spectrum Observed, *Science* **1999**, *284*, 135-137.

(9) Marx, D; Hutter, J. *Ab Initio* Molecular Dynamics: Theory and Implementation, In Modern Methods and Algorithms of Quantum Chemistry, Grotendorst, J., Ed.; NIC; FZ Julich: Julich, Germany, **2000**; 301-449.

(10) Vendrell, O.; Gatti, F.; Lauvergnat, D.; Meyer, H. D. Full-Dimensional (15-Dimensional) Quantum-Dynamical Simulation of the Protonated Water Dimer. I. Hamiltonian Setup and Analysis of the Ground Vibrational State. *J. Chem. Phys.,* **2007**, *127*, 184302.

(11) Vendrell, O.; Gatti, F.; Meyer, H. D. Dynamics and Infrared Spectroscopy of the Protonated Water Dimer. *Angew. Chem., Int. Ed.,* **2007**, *46*, 6918-6921.

(12) Vendrell, O.; Gatti, F.; Meyer, H. D.; Strong Isotope Effects in the Infrared Spectrum of the Zundel Cation. *Angew. Chem., Int. Ed.,* **2009**, *48*, 352-355.

(13) Hooper, R.; Boutwell, D.; Kaledin, M. Assignment of Infrared-Active Combination Bands in the Vibrational spectra of Protonated Molecular Clusters Using Driven Classical Trajectories: Applications to N_4H^+ and N_4D^+. *J. Phys Chem. A,* **2019,** *123*, 5613-5620.

(14) Botschwina, P.; Dutoi, T.; Mladenovic, M.; Oswald, R.; Schmatz, S.; Stoll, H. Theoretical Investigations of Proton-Bound Cluster Ions. *Faraday Discuss*. **2001**, *118*, 433-453.

(15) Terrill, K.; Nesbitt, D.J. *Ab initio* Anharmonic Vibrational Frequency Predictions for Linear Proton-Bound Complexes $OC–H^+–CO$ and $N_2–H^+–N_2$. *Phys. Chem. Chem. Phys*. **2010**, *12*, 8311-8322.

(16) Liao, H. Y.; Tsuge, M.; Tan, J. A.; Kuo, J. L.; Lee, Y. P. Infrared Spectra and Anharmonic Coupling of Proton-Bound Nitrogen Dimers N_2-H^+-N_2, N_2-D^+-N_2, and $^{15}N_2$-H^+-$^{15}N_2$ in Solid Para-Hydrogen. *Phys. Chem. Phys. Chem.* **2017**, *19*, 20484-20492.

(17) Yu, Q.; Bowman, J. M.; Fortenberry, R. C.; Mancini, J. S.; Lee, T. J.; Crawford, T. D.; Klemperer, W.; Francisco, J. S. Structure, Anharmonic Vibrational Frequencies, and Intensities

of $NNHNN^+$. *J. Phys. Chem. A* **2015**, *119*, 11623-11631.

(18) Ricks, A. M.; Douberly, G. E.; Duncan, M. A. Infrared Spectroscopy of the Protonated Nitrogen Dimer: The Complexity of Shared Proton Vibrations. *J. Chem. Phys.* **2009**, *131*, 1045312.

(19) Fortenberry, R. C.; Yu, Q.; Bowman, J. M.; Lee, T. J.; Crawford, T. D.; Klemperer, W. F.; Francisco, J. S. Communication: Spectroscopic consequences of proton delocalization in $OCHCO^+$, *J. Chem. Phys.* **2015**, *143*, 071102.

(20) Cotton, C. E.; Francisco, J. S.; Linguerri, R.; Mitrushchenkov, A. O. Structural and Spectroscopic Study of the van der Waals Complex of CO with HCO^+ and the Isoelectronic Complex of CS with HCS^+. *J. Chem. Phys.*, **2012**, *136*, 184307.

(21) Pandey, A.; Poirier, B. Using Phase-Space Gaussians to Compute the Vibrational States of $OCHCO^+$. *J. Chem. Phys.* **2019**, *151*, 014114.

(22) Begum, S.; Subramanian, R. A Theoretical Investigation of the Energetics and Spectroscopic Properties of the Gas-Phase Linear Proton-Bound Cation-Molecule Complexes, XCH^+-N_2 (X=O, S). *J. Mol. Model.,* **2016**, *22*, 6.

(23) Fortenberry, R. C.; Francisco, J. S.; Lee, T. J. Toward the Astronomical Detection of the Proton-Bound Complex NN-HCO^+: Implications for the Spectra of Protoplanetary Discs. *Astrophys. J.* **2016**, *819,* 141.

(24) Fortenberry, R. C.; Lee, T. J.; Francisco, J. S. Quantum Chemical Analysis of the CO–HNN^+ Proton-Bound Complex. *J. Phys. Chem. A* **2016**, *120*, 7745-7752.

(25) Yao, Q.; Xie, C.; Guo, H. Competition Between Proton Transfer and Proton Isomerization in the N_2 + HOC^+ Reaction on an *Ab Initio*-Based Global Potential Energy Surface. *J. Phys. Chem. A* **2019**, *123*, 5347-5355.

(26) Mladenović, M.; Roueff, E. Ion-Molecule Reactions Involving HCO^+ and N_2H^+: Isotopologue Equilibria from New Theoretical Calculations and Consequences for Interstellar Isotope Fractionation. *Astron. Astrophys.* **2014**, *566,* A144.

(27) Verdes, D.; Linnartz, H.; Maier, J.P.; Botschwina, P.; Oswald, R.; Rosmus, P.; Knowles, P. J. Spectroscopic and Theoretical Characterization of Linear Centrosymmetric NN..H+..NN. *J. Chem. Phys*. **1999**, *111*, 8400-8403.

(28) Smith, D. The Ion Chemistry of Interstellar Clouds. *Chem. Rev*. **1992**, *92*, 1473-1485.

(29) Herbst, E.; Payzant, J.; Schiff, H.; Bohme, D. Rate of the Reaction N_2H^+ + CO Yields HCO^+ + N_2 and its Significance for the Interstellar Chemistry of N_2H^+. *Astrophys. J.* **1975**, *201*, 603-606.

(30) Woods, R. C.; Gudeman, C. S.; Dickman, R. L.; Goldsmith, P. F.; Huguenin, G. R.; Irvine, W. M.; Hjalmarson, A.; Nyman, L. A.; Olofsson, H. The $[HCO^+]/[HOC^+]$ Abundance Ratio in Molecular Clouds, *Astrophys. J*. **1983**, *270*, 583−588.

(31) Ziurys, L. M.; Apponi, A. J. Confirmation of Interstellar HOC^+: Reevaluating the $[HCO^+]/[HOC^+]$ Abundance Ratio. *Astrophys. J.* **1995**, *455*, L73−L76.

(32) McGuire, B.A. 2018 Census of Interstellar, Circumstellar, Extragalactic, Protoplanetary Disk, and Exoplanetary Molecules, *Astrophys J. Suppl. S.* **2018**, *239,* 17 (48pp).

(33) Vigren, E.; Zhaunerchyk, V.; Hamberg, M.; Kaminska, M.; Semaniak, J.; Ugglas, M. af; Larsson, M.; Thomas, R. D.; Geppert, W. D. Reassessment of the Dissociative Recombination of N_2H^+ at Cryring. *Astrophys. J.* **2012**, *757*, 34 (4pp).

(34) Lique F.; Daniel, F.; Pagani L.; Feautrier N. Hyperfine Excitation of N_2H^+ by H_2: Towards a Revision of N_2H^+ Abundance in Cold Molecular Clouds. *MNRAS* **2015**, *446*, 1245–1251.

(35) Ferriere, K.M. The Interstellar Environment of our Galaxy. *Rev. Mod. Phys.,* **2001**, *73*, 1031-1066.

(36) Perrin, C. L.; Nielson, J. B. "Strong" Hydrogen Bonds in Chemistry and Biology, *Ann. Rev. Phys. Chem.* **1997**, *48*, 511-544.

(37) Bergin, E. A.; Alves, J.; Huard, T.; Lada, C. L. N_2H^+ and $C^{18}O$ Depletion in a Cold Dark Cloud. *Astrophys. J.* **2002**, *570*, L101-L104.

(38) Werner, H. J.; Adler, T. B.; Manby, F. R. General orbital invariant MP2-F12 theory. *J. Chem. Phys.* **2007***, 126*, 164102.

(39) Adler, T. B.; Knizia G.; Werner, H. J. A Simple and Efficient CCSD(T)-F12 Approximation *J. Chem. Phys*. **2007**, *127*, 221106.

(40) Knizia, G.; Adler, T. B.; Werner, H. J. Simplified CCSD(T)-F12 Methods: Theory and Benchmarks, *J. Chem. Phys.* **2009**, *130*, 054104.

(41) Jakubikova, E.; Rappe A.K.; Bernstein, E.R. Exploration of Basis Set Issues for Calculation of Intermolecular Interactions, *J. Phys. Chem. A* **2006,** *110,* 9529–9541.

(42) Martin, J. M. L.; Kesharwani, M. K. Assessment of CCSD(T)-F12 Approximations and Basis Sets for Harmonic Vibrational Frequencies*, J. Chem. Theory Comput.* **2014**, *10*, 2085−2090.

(43) Sirianni, D. A.; Burns, L. A.; Sherrill, C. D. Comparison of Explicitly Correlated Methods for Computing High-Accuracy Benchmark Energies for Noncovalent Interactions, *J. Chem. Theory Comput*. **2017**, *13*, 86−99.

(44) Kaledin, M.; Kaledin, A. L.; Bowman, J. M. Vibrational Analysis of the $H_5O_2^+$ Infrared Spectrum Using Molecular and Driven Molecular Dynamics, *J. Phys. Chem. A* **2006**, *110,* 2933-2939.

(45) Bowman, J. M.; Zhang, X. B.; Brown, A. Normal-Mode Analysis Without the Hessian: A Driven Molecular-Dynamics Approach, *J. Chem. Phys*. **2003**, *119*, 646-650.

(46) Kaledin, M.; Brown, A.; Kaledin, A. L. Normal Mode Analysis Using the Driven Molecular Dynamics Method. II. An Application to Biological Macromolecules, *J. Chem. Phys*. **2004**, *121*, 5646 -5653.

(47) Kaledin, M.; Kaledin, A. L.; Brown, A.; Bowman, J. M. In Normal Mode Analysis: Theory and Applications to Biological and Chemical Systems. Cui, Q.; Bahar, I., Eds. CRC Press: **2006**.

(48) Györffy, W.; Knizia, G.; Werner, H. J. Analytical Energy Gradients for Explicitly Correlated wave functions. I. Explicitly Correlated Second-Order Møller-Plesset Perturbation Theory. *J. Chem. Phys*. **2017**, *147*, 214101.

(49) Györffy, W.; Werner, H. J. Analytical Energy Gradients for Explicitly Correlated Wave Functions. II. Explicitly Correlated Coupled Cluster Singles and Doubles with Perturbative Triples Corrections: CCSD(T)-F12., *J. Chem. Phys.* **2018**, *148*, 114104.

(50) Swope, W.C.; Andersen, H.C.; Berens, P.H.; Wilson, K.R. A Computer Simulation Method for the Calculation of Equilibrium Constants for the Formation of Physical Clusters of Molecules: Application to Small Water Clusters, *J. Chem. Phys*. **1982**, *76* ,637-649.

(51) MOLPRO, version 2019.2, a package of ab initio programs, Werner, H. J.; Knowles, P. J.; Knizia, G.; Manby, F. R.; Schütz, M.; Celani, P.; Györffy, W.; Kats, D.; Korona, T.; Lindh, R.; Mitrushenkov, A.; Rauhut, G.; Shamasundar, K. R.; Adler, T. B.; Amos, R. D.; Bennie, S. J.; Bernhardsson, A.; Berning, A.; Cooper, D. L.; Deegan, M. J. O.; Dobbyn, A. J.; Eckert, F.; Goll, E.; Hampel, C.; Hesselmann, A.; Hetzer, G.; Hrenar, T.; Jansen, G.; Köppl, C.; Lee, S. J. R.; Liu, Y.; Lloyd, A. W.; Ma, Q.; Mata, R. A.; May, A. J.; McNicholas, S. J.; Meyer, W.; Miller III, T. F.; Mura, M. E.; Nicklass, A.; O'Neill, D. P.; Palmieri, P.; Peng, D.; Pflüger, K.; Pitzer, R.;

Reiher, M.; Shiozaki, T.; Stoll, H.; Stone, A. J.; Tarroni, R.; Thorsteinsson, T.; Wang, M.; and Welborn, M. see https://www.molpro.net.

(52) Kaledin, M.; Wood, C. A. *Ab Initio* Studies of Structural and Vibrational Properties of Protonated Water Cluster $H_7O_3^+$ and Its Deuterium Isotopologues: An Application of Driven Molecular Dynamics, *J. Chem. Theory Comput*. **2010***, 6*, 2525-2535.

(53) Berens, P. H.; Wilson, K. R.; Molecular Dynamics and Spectra .1. Diatomic Rotation and Vibration, *J. Chem. Phys.* **1981**, *74*, 4872-4882.

(54) Kaledin, M.; Kaledin, A. L.; Bowman, J. M.; Dong, J.; Jordan, K. D. Calculation of the Vibrational Spectra of $H_5O_2^+$ and its Deuterium-Substituted Isotopologues by Molecular Dynamics Simulations. *J. Phys. Chem. A* **2009**, *113*, 7671-7677.

(55) Demtröder, W. Laser Spectroscopy: Vol. 1: Basic Principles, Springer Science, **2008**.

(56) Huang, X. C.; Braams, B. J.; Bowman, J. M. *Ab Initio* Potential Energy and Dipole Moment Surfaces for $H_5O_2^+$. *J. Chem. Phys.* **2005**, *122*, 044308.

(57) Huang, X. C.; Braams, B. J.; Bowman J. M. *Ab Initio* Potential Energy and Dipole Moment Surfaces of $(H_2O)_2$. *J Phys Chem A* **2006**, *110*, 445-451.

(58) Yu, Q.; Bowman, J. M. Communication: VSCF/VCI Vibrational Spectroscopy of $H_7O_3^+$ and $H_9O_4^+$ Using High-Level, Many-Body Potential Energy Surface and Dipole Moment Surfaces. *J. Chem. Phys.,* **2017**, *146*, 121102.

(59) Rauhut, G.; Hrenar, T. A Combined Variational and Perturbational Study on the Vibrational Spectrum of P_2F_4. *Chem. Phys.* **2008**, *346*, 160-166.

(60) Neff, M.; Rauhut, G. Toward Large Scale Vibrational Configuration Interaction Calculations. *J. Chem. Phys*. **2009**, *131*, 124129.

(61) Neff, M.; Hrenar, T.; Oschetzki, D.; Rauhut, G. Convergence of Vibrational Angular Momentum Terms within the Watson Hamiltonian, *J. Chem. Phys*. **2011**, *134*, 064105.

(62) Lovas, F.J.; Coursey, J. S.; Kotochigova, S. A.; Chang, J.; Olsen, K.; R. A. Dragoset, R. A. NIST Physical Measurement Laboratory. Triatomic Spectral Database, **2003**, https://www.nist.gov/pml/triatomic-spectral-database.

(63) Gaussian 16, Revision A.03, Frisch, M. J.; Trucks, G. W.; Schlegel, H. B.; Scuseria, G. E.; Robb, M. A.; Cheeseman, J. R.; Scalmani, G.; Barone, V.; Petersson, G. A.; Nakatsuji, H.; Li, X.; Caricato, M.; Marenich, A. V.; Bloino, J.; Janesko, B. G.; Gomperts, R.; Mennucci, B.; Hratchian, H. P.; Ortiz, J. V.; Izmaylov, A. F.; Sonnenberg, J. L.; Williams-Young, D.; Ding, F.; Lipparini, F.; Egidi, F.; Goings, J.; Peng, B.; Petrone, A.; Henderson, T.; Ranasinghe, D.; Zakrzewski, V. G.; Gao, J.; Rega, N.; Zheng, G.; Liang, W.; Hada, M.; Ehara, M.; Toyota, K.; Fukuda, R.; Hasegawa, J.; Ishida, M.; Nakajima, T.; Honda, Y.; Kitao, O.; Nakai, H.; Vreven, T.; Throssell, K.; Montgomery, J. A., Jr.; Peralta, J. E.; Ogliaro, F.; Bearpark, M. J.; Heyd, J. J.; Brothers, E. N.; Kudin, K. N.; Staroverov, V. N.; Keith, T. A.; Kobayashi, R.; Normand, J.; Raghavachari, K.; Rendell, A. P.; Burant, J. C.; Iyengar, S. S.; Tomasi, J.; Cossi, M.; Millam, J. M.; Klene, M.; Adamo, C.; Cammi, R.; Ochterski, J. W.; Martin, R. L.; Morokuma, K.; Farkas, O.; Foresman, J. B.; Fox, D. J. Gaussian, Inc., Wallingford CT, 2016.

(64) Fortenberry, R. C.; Huang, X.; Yachmenev, A.; Thiel, W.; Lee, T. J. On the Use of Quartic Force Fields in Variational Calculations. *Chem. Phys. Lett.* **2013**, *574*, 1-12.

Supporting Information

Analysis of the Proton Transfer Bands in the Infrared Spectra of Linear N_2H^+…OC and N_2D^+…OC Complexes Using Electric Field-Driven Classical Trajectories

Dalton Boutwell, Onyi Okere, Oluwaseun Omodemi, Alexander Toledo, Antonio Barrios, Monique Olocha, Martina Kaledin*

Department of Chemistry & Biochemistry, Kennesaw State University, 370 Paulding Ave NW, Box # 1203, Kennesaw, GA 30144

This document contains additional information on implementation of the driven molecular dynamics method (**Scheme S1**). Structural parameters, dipole moments, and harmonic vibrational frequencies of N_2H^+…OC and N_2D^+…OC at MP2, MP2-F12, CCSD(T), CCSD(T)-F12 with aug-cc-pVDZ (AVDZ) and aug-cc-pVDZ (AVTZ) levels of theory are listed in **Tables 1S-2S.** The T-shaped transition state was also found and the CO rotational barrier predicted (**Table 3S**). The dissociation energies D_e for the process N_2H^+…OC $\rightarrow$ N_2H^+ + CO at various levels of theory are listed in **Table 4S**. VCI overtones and combination bands are shown in **Table 5S** and compared to the previous calculations at the VPT2 level of theory.[24] **Figure 1S** shows that the DMD MP2-F12/AVDZ and CCSD(T)-F12/AVDZ simulations produce very similar absorption profiles and internal coordinate excitation signatures for the parallel H^+ transfer vibration. These findings rationalize running the extremely time-consuming DMD scans at the lower level of theory, MP2-F12/AVDZ, to assign the vibrational spectra. Average absorbed energies and atomic coordinates along the DMD MP2-F12/AVDZ trajectories are visualized on **Figures 2S-4S.**

Corresponding Author
*Email: mkaledin@kennesaw.edu (M.K.)

The potential and field energy gradients are computed on-the-fly along the trajectory. Direct differentiation of the dipole's three components with respect to the nuclear Cartesian coordinates is time consuming and unnecessary. The scheme below shows that only the parallel component contributes to the energy.

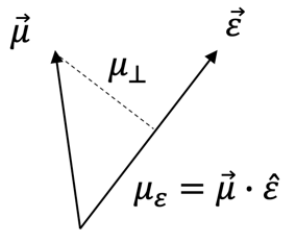

Scheme S1. Decomposition of the dipole into parallel and perpendicular components of the electric field.

Table S1. Interatomic Distances R (in Å), Dipole Moments (atomic units), and Harmonic Vibrational Frequencies (in cm^{-1}) of $CO\ldots HNN^{+}$. ($C_{\infty v}$ symmetry)

	MP2 AVDZ	MP2-F12 AVDZ	MP2 AVTZ	CCSD(T) AVDZ	CCSD(T)-F12 AVDZ	CCSD(T) AVTZ
R(N–N)	1.1255	1.1192	1.1090	1.1151	1.1075	1.0992
R(N–H)	1.1085	1.1085	1.1027	1.1109	1.1085	1.1042
R(O–H)	1.4750	1.4679	1.4650	1.4709	1.4661	1.4602
R(C–O)	1.1592	1.1540	1.1491	1.1591	1.1534	1.1487
μ_e (a.u.)	0.8694	0.8472	0.8534	0.8234	0.8094	0.8087
ω_1 (σ)	2472	2477	2477	2544	2573	2556
ω_2 (σ)	2030	2050	2060	2054	2079	2080
ω_3 (σ)	1927	1929	1925	1950	1960	1947
ω_4 (π)	974	956	1028	981	962	1039
ω_5 (σ)	264	265	269	265	264	271
ω_6 (π)	196	192	211	198	195	214
ω_7 (π)	102	96	101	104	99	103

Table S2. Harmonic Vibrational Frequencies (in cm^{-1}) of $CO\ldots DNN^{+}$. ($C_{\infty v}$ symmetry)

	MP2 AVDZ	MP2-F12 AVDZ	MP2 AVTZ	CCSD(T) AVDZ	CCSD(T)-F12 AVDZ	CCSD(T) AVTZ
ω_1 (σ)	2309	2336	2335	2445	2484	2467
ω_2 (σ)	2022	2042	2054	2024	2053	2058
ω_3 (σ)	1502	1490	1486	1494	1492	1480
ω_4 (π)	718	707	761	723	711	790
ω_5 (σ)	261	262	265	262	261	267
ω_6 (π)	192	188	206	194	191	209
ω_7 (π)	102	95	100	103	98	102

Table 3S. Interatomic Distances R (in Å), Rotational Energy Barrier (relative to the N_2H^+…OC minimum) and its Zero-Point Energy Corrected Value (in cm^{-1}), and Harmonic Vibrational Frequencies (in cm^{-1}) of the N_2H^+…OC T-shaped transition state corresponding to the CO rotation (C_s symmetry)

	MP2 AVDZ	MP2-F12 AVDZ	MP2 AVTZ	CCSD(T) AVDZ	CCSD(T)-F12 AVDZ	CCSD(T) AVTZ
R(C–O)	1.1539	1.1493	1.1426	1.1495	1.1435	1.1382
R(X–H)[a]	2.0480	2.0454	2.0366	2.0931	2.0889	2.0772
R(N–H)	1.0605	1.0587	1.0516	1.0588	1.0559	1.0495
R(N–N)	1.1253	1.1189	1.1086	1.1151	1.1074	1.0991
Barrier height	3372	3297	3350	3885	3791	3833
ZPE corr. value	3211	3159	3220	3747	3673	3728
ω_1 (A')	256i	256i	251i	261i	262i	258i
ω_2 (A')	100	92	99	97	89	94
ω_3 (A")	128	113	123	126	111	120
ω_4 (A')	138	136	144	135	132	139
ω_5 (A')	628	628	711	612	613	705
ω_6 (A")	708	691	776	688	675	769
ω_7 (A')	2037	2060	2074	2082	2115	2122
ω_8 (A')	2094	2124	2123	2237	2274	2258
ω_9 (A')	3082	3088	3100	3125	3142	3146

[a] X is the center of mass of the CO bond.

Table S4. $CO\cdots HNN^+ \rightarrow N_2H^+ + CO$ Dissociation Energies, D_e (in cm^{-1}) and Zero Point Energy Corrected Values, D_0 (in cm^{-1})

Method	D_e	D_0
MP2/AVDZ	4663	4417
MP2-F12/AVDZ	4395	4211
MP2/AVTZ	4615	4414
CCSD(T)/AVDZ	5096	4858
CCSD(T)-F12/AVDZ	4814	4634
CCSD(T)/AVTZ	4997	4810

Table S5. MP2-F12/AVDZ Overtones and Combination bands for N_2H^+…OC and N_2D^+…OC

	N_2H^+…OC		N_2D^+…OC	
Mode	VCI[a]	VPT2[b]	VCI[a]	VPT2[b]
$2\nu_4$	1902	2761.0	1415	1946.1
$2\nu_5$	547	583.5	522	568.4
$2\nu_6$	428	586.3	414	554.6
$2\nu_7$	282	334.1	279	312.5
$\nu_1+\nu_5$	2574	2741.1	2545	2704.9
$\nu_1+\nu_6$	2420	2686.3	2570	2675.6
$\nu_1+\nu_7$	2366	2556.6	2494	2553.9
$\nu_2+\nu_5$	2334	2352.5	2292	2347.5
$\nu_2+\nu_6$	2243/2235	2349.4	2221	2323.5
$\nu_2+\nu_7$	2153	2220.7	2140	2201.1
$\nu_3+\nu_4$	2474	3004.1	1916	2180.3
$\nu_3+\nu_5$	1924	1948.2	1570	1563.7
$\nu_3+\nu_6$	1784	1951.4	1440	1528.8
$\nu_3+\nu_7$	1676	1811.5	1352	1390.6
$\nu_4+\nu_5$	1241	1593.1	988	1194.7
$\nu_4+\nu_6$	1162/1174/1185	1608.6	913/924/931	1194.1
$\nu_4+\nu_7$	1085/1096/1090	1479.7	843/847	1067.5
$\nu_5+\nu_6$	505	581	481	556.6
$\nu_5+\nu_7$	421	456.8	402	436.3
$\nu_6+\nu_7$	356/367	450.2	341/354	421.4

[a]Modes mixing was observed in some cases.

[b]From reference 24.

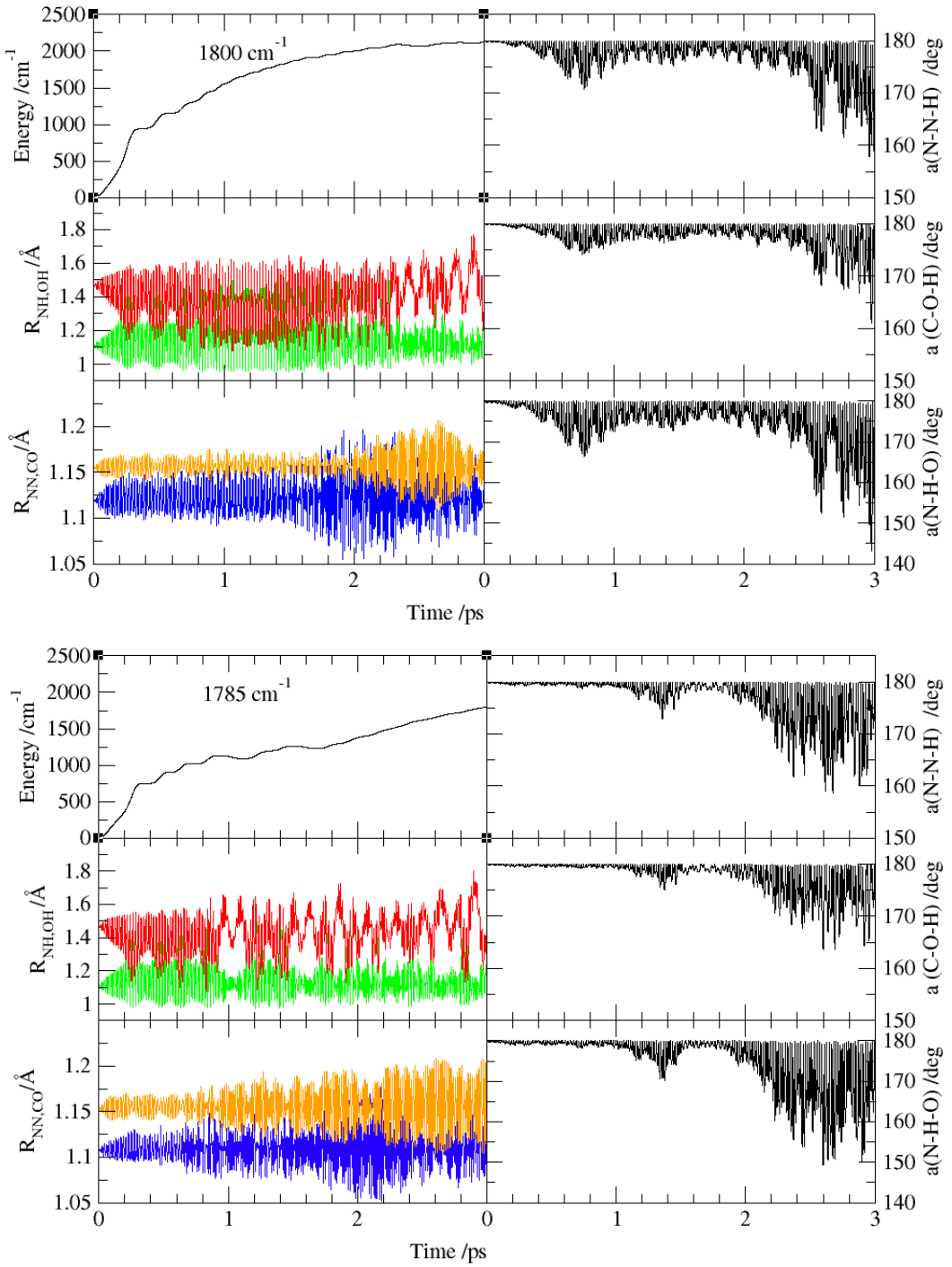

Figure 1S. The DMD analysis of the H^+ parallel stretch vibration at the MP2-F12/AVDZ (1800 cm^{-1}) and CCSD(T)-F12/AVDZ (ν_3=1785 cm^{-1}) levels of theory. Average absorbed energy is in cm^{-1}, interatomic distances are in Å (OH in red, NH in green, CO in orange, and NN in blue), and bond angles in degrees. The intensity of the electric field was 75 mV/bohr.

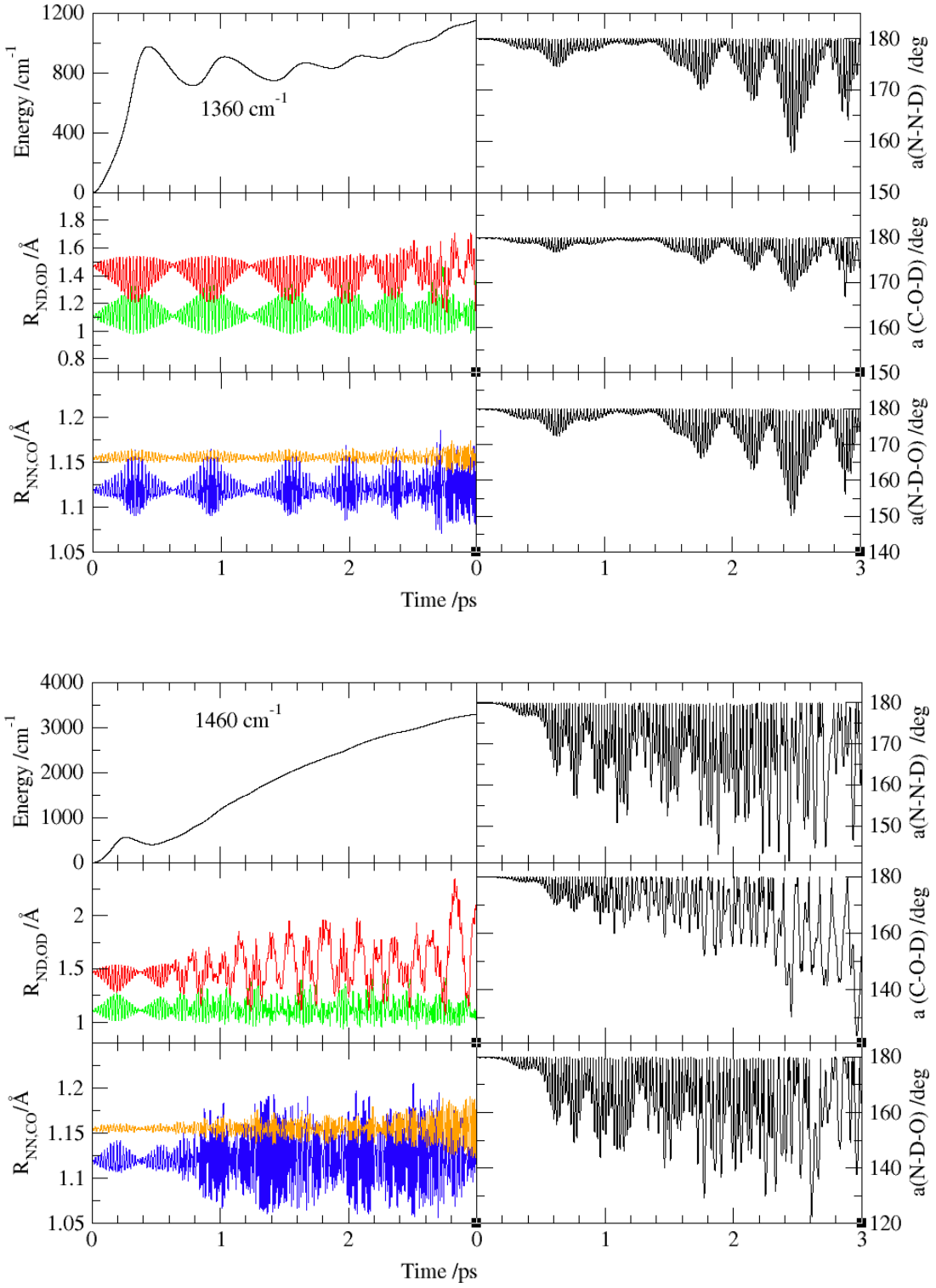

Figure 2S. The DMD MP2-F12/AVDZ analysis for the N_2D^+ …OC driven frequencies ν_3=1360 cm^{-1} and $2\nu_4$=1460 cm^{-1}. Average absorbed energy is in cm^{-1}, interatomic distances are in Å (OD in red, ND in green, CO in orange, and NN in blue), and bond angles in degrees. The intensity of the electric field was 75 mV/bohr.

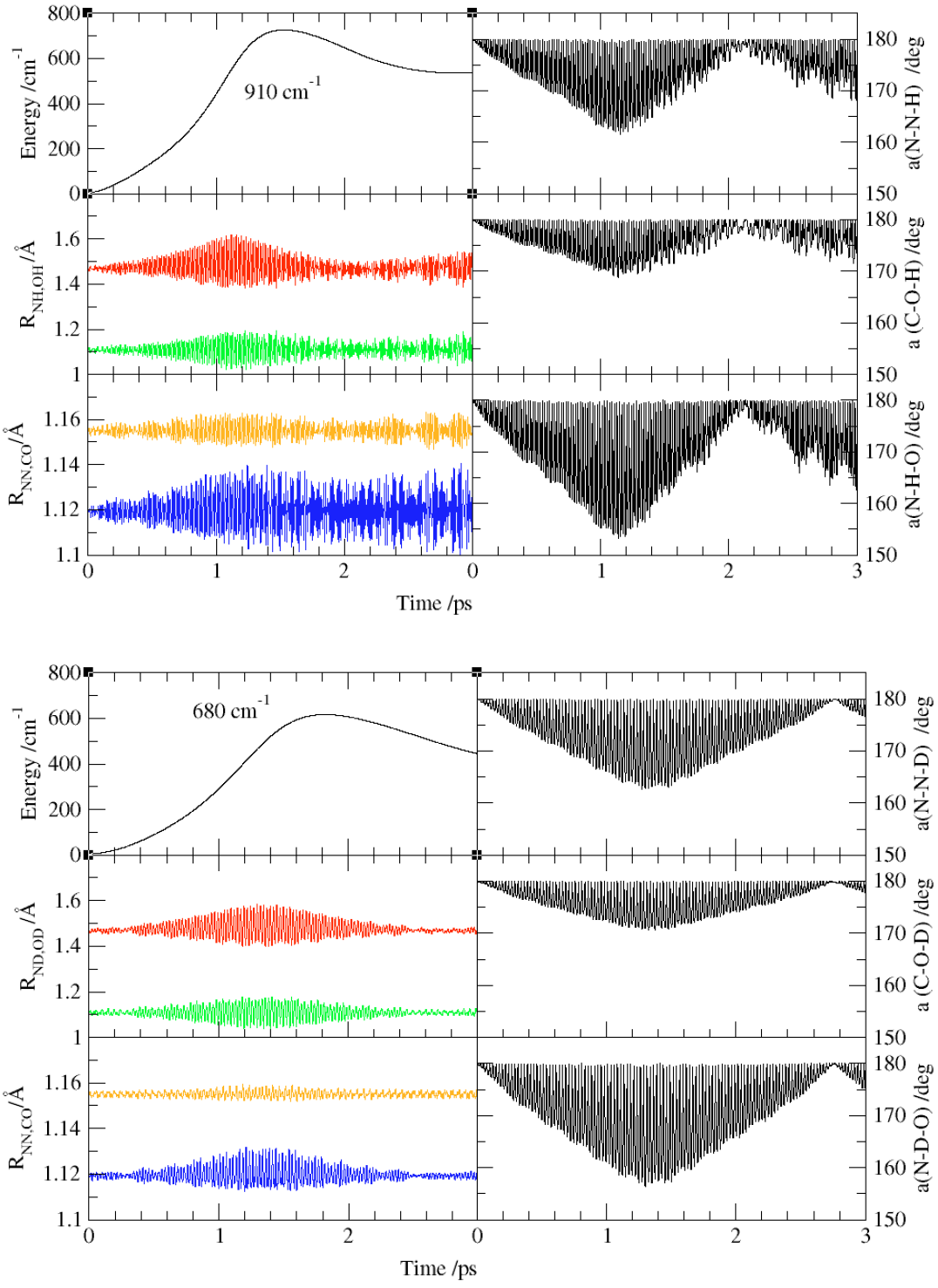

Figure 3S. DMD MP2-F12/AVDZ analysis for the N_2H^+ …OC driven frequencies ν_4=910 cm^{-1} (top panel) and N_2D^+…OC ν_4=680 cm^{-1} (bottom panel). Average absorbed energy is in cm^{-1}, interatomic distances are in Å (OH/OD in red, NH/ND in green, CO in orange, and NN in blue), and bond angles in degrees. The intensity of the electric field was 75 mV/ bohr.

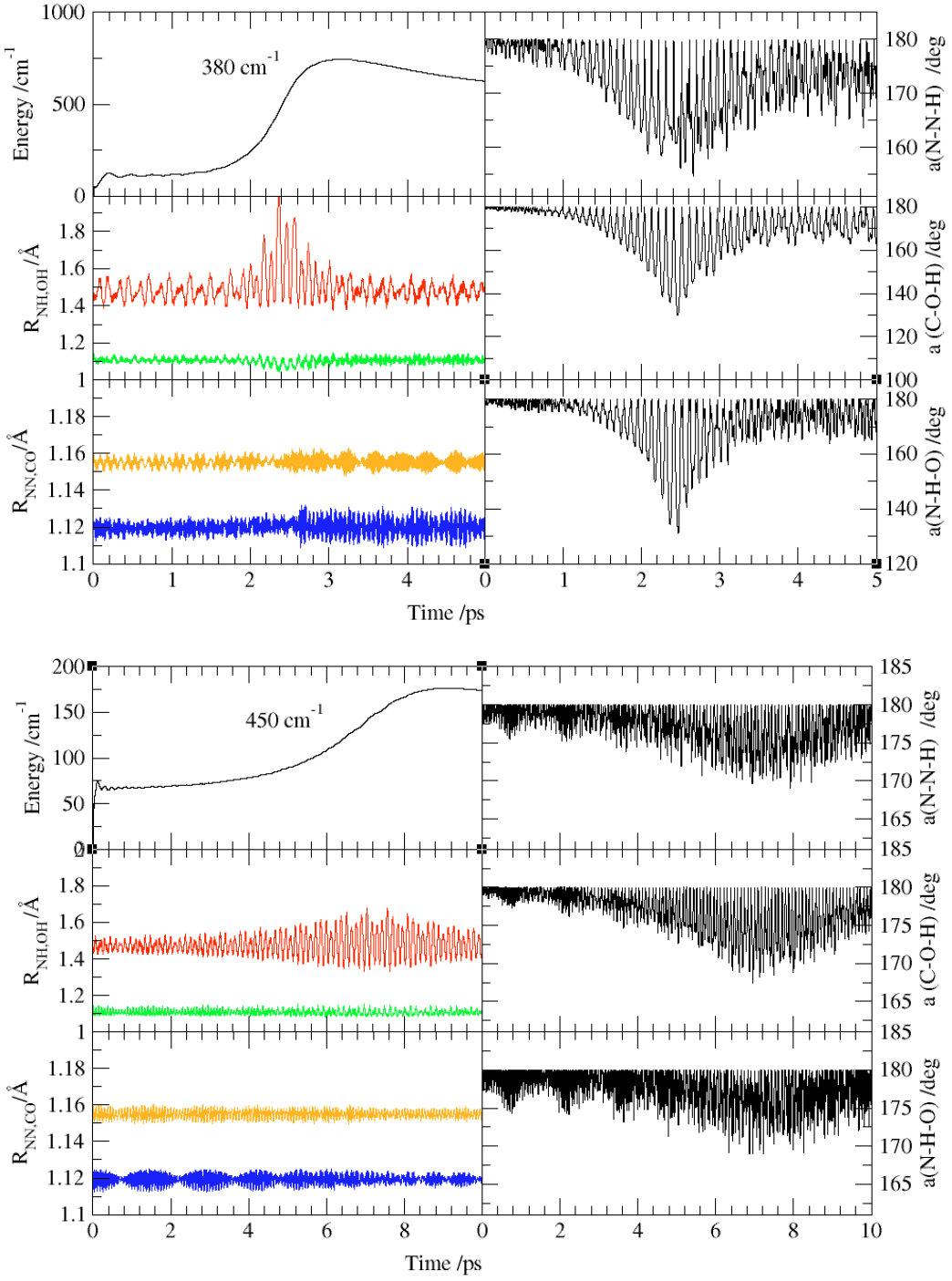

Figure 4S. DMD MP2-F12/AVDZ analysis for the N_2H^+ …OC combination bands $\nu_5+\nu_7$=380 cm^{-1} and $\nu_5+\nu_6$=450 cm^{-1} . Average absorbed energy is in cm^{-1}, interatomic distances are in Å (OH in red, NH in green, CO in orange, and NN in blue), and bond angles are in degrees. The intensities of the electric field for two combination bands were 150 and 200 mV/bohr, respectively.